ISSN 1560-3547, Regular and Chaotic Dynamics, 0000, Vol. 00, No. 0, pp. 1–22. © RCD Editorial Office, 2016.

Three-dimensional quasi-geostrophic staggered vortex arrays

Jean N. Reinaud[1*]

[1] *University of St Andrews*
Mathematical Institute, North Haugh, St Andrews, UK

Received August 17, 2017; revised Month XX, 20XX; accepted Month XX, 20XX

Abstract—We determine and characterise relative equilibria for arrays of point vortices in a three-dimensional quasi-geostrophic flow. The vortices are equally spaced along two horizontal rings whose centre lies on the same vertical axis. An additional vortex may be placed along this vertical axis. Depending on the parameters defining the array, the vortices on the two rings are of equal or opposite sign. We address the linear stability of the point vortex arrays. We find both stable equilibria and unstable equilibria, depending on the geometry of the array. For unstable arrays, the instability may lead to the quasi-regular or to the chaotic motion of the point vortices. The linear stability of the vortex arrays depends on the number of vortices in the array, on the radius ratio between the two rings, on the vertical offset between the rings and on the vertical offset between the rings and the central vortex, when the latter is present. In this case the linear stability also depends on the strength of the central vortex. The nonlinear evolution of a selection of unstable cases is presented exhibiting examples of quasi-regular motion and of chaotic motion.
editorial@rcd.ru.

MSC2010 numbers: 76B47,76E20

DOI: 10.0000/S1560354700000012

Keywords: Quasi-geostrophy, point vortex dynamics, equilibria, vortex arrays

INTRODUCTION

Arrays of point vortices have been investigated nearly as early as Helmholtz (1858) [1] derived the equations governing flows with vorticity. Kirchhoff [2] first introduced the notion of a point vortex where the vortex circulation is locally concentrated on a Dirac distribution. Configurations of two-dimensional point vortices in mutual equilibrium were identified by Thomson (Lord Kelvin) [4]. At this stage, we should mention analogous works on floating magnets [5] which motivated the study of arrays of vortices in mutual equilibrium. The linear stability of circular arrays of two-dimensional point vortices was addressed by J. J. Thomson in 1883 [6]. The problem was later revisited by Haverlock (1931)[7], Moser (1935) [8], Khazin (1976) [9] and by Mertz (1978) [10].

In the context of large-scale oceanic vortices, the flow dynamics is strongly influenced by the background planetary rotation as well as the stable density stratification. When these effects are dominant, the flow remains close to both geostrophic and hydrostatic balance whereby the horizontal pressure forces are (approximately) balanced by the Coriolis forces and the vertical pressure force is (approximately) balanced by the gravitational force. In such geophysical environments, the existence and the stability of vortex arrays were first studied in a shallow water model by Stewart (1943, 1945) [11, 12], and in more detail by Morikawa and Svenson (1971) [13]. In the latter study, the influence of a central vortex on the stability of the vortex array was also considered. Following these early studies, a vast body of literature has extended the results on the stability of point vortex arrays [14–29] as well as finite core vortex arrays e.g. [30–33]. Additionally, Sokolovskiy *et al.* (2020) [34] have recently studied the evolution of non-equilibrium four-vortex arrays in a two-layer quasi-geostrophic system.

*E-mail: jean.reinaud@st-andrews.ac.uk

Reinaud (2019) [35] studied vortex arrays in a three-dimensional quasi-geostrophic flow under the Boussinesq approximation, relevant to oceanic applications. Both point vortices and finite volume vortices were considered in the study. It was shown that an array consisting of a single ring of $n \leq 5$ vortices is linearly neutrally stable. Arrays of $n > 5$ vortices are unstable. This is in contrast to the classical result for two-dimensional vortices where the array is stable for $n \leq 7$. A like-signed central vortex may however stabilise the array for a larger number of vortices in both cases. Such vortex arrays may natural emerge from the destabilisation of circular shear zones, see [36]. More recently, Dritschel (2021) has extended the study by considering arrays of point vortices along a single ring in an exponential density stratification, relevant to atmospheric applications.

During the nonlinear evolution of vortex arrays with an even number of vortices, the vortices may become staggered. Every other vortex moves inward (resp. outward) to re-organise the array, albeit temporarily, into an array of vortices staggered onto two rings of different radius. Dritschel (2021) [37] presented examples of equilibria for staggered vortices but has not formally addressed their linear stability.

In the present paper, we study arrays of point vortices in mutual equilibrium where the point vortices are distributed along two rings with, possibly, an additional central vortex. We show the existence of relative equilibria and we study their linear stability. Equilibria are often unstable but there also exist regions of the parameter space where the arrays are robust and may stably persist. Thus, the study justifies, in an idealised set-up, the possible existence of robust vortex configuration in rotating and stratified fluids, such as the storm clusters recently observed over the poles of Jupiter by [41]. We also present examples of the evolution of various unstable vortex arrays.

1. THE MODEL

1.1. The quasi-geostrophic approximation

The quasi-geostrophic (QG) model is the simplest dynamical model which takes into account, at leading order, the effects of the rapid background planetary rotation and of the stable background density stratification. In the context of the present study, the model is obtained by a Rossby number expansion of the full three-dimensional rotating stratified Euler's equations under the Boussinesq approximation. A detailed derivation of the quasi-geostrophic model can be found in [38]. The QG model is strictly valid when $Fr^2 \ll Ro \ll 1$, where $Fr = U/(NH)$ is the Froude number and $Ro = U/(fL)$. Here, U is a characteristic horizontal velocity scale, H and L are characteristic vertical and horizontal scales respectively, N is the buoyancy frequency and f is the Coriolis frequency. For simplicity we assume both N and f are constant and we rescale the physical vertical coordinate z_p by the constant ratio N/f, i.e. $z = Nz_p/f$, while the two horizontal coordinates x, y remain unchanged. The ratio N/f is typically large at mid-latitudes, hence in practice the physical vertical direction is stretched in the rescaled coordinate system (x, y, z). In this system, the potential vorticity anomaly q (hereinafter referred to as PV for simplicity) the Laplacian of a stream function φ,

$$q = \boldsymbol{\nabla}^2\varphi = \frac{\partial^2\varphi}{\partial y^2} + \frac{\partial^2\varphi}{\partial y^2} + \frac{\partial^2\varphi}{\partial z^2}. \tag{1.1}$$

At leading order in Ro the advecting velocity field is a layer-wise two-dimensional divergence-free field given by

$$u = -\frac{\partial\varphi}{\partial y}, \quad v = \frac{\partial\varphi}{\partial x}. \tag{1.2}$$

Strictly speaking the vertical velocity w is not zero in the QG model but is too small to contribute to the advection at the order in Ro considered. In the absence of frictional and diabatic effects, and for a constant Coriolis frequency, the PV is materially conserved,

$$\frac{\mathrm{D}q}{\mathrm{D}t} = \frac{\partial q}{\partial t} + u\frac{\partial q}{\partial x} + v\frac{\partial q}{\partial y} = 0. \tag{1.3}$$

Equation (1.1) can be formally inverted to find φ from q,

$$\varphi(\boldsymbol{x}) = \iiint G(\boldsymbol{x}-\boldsymbol{x'})\, q(\boldsymbol{x'})\, \mathrm{d}^3\boldsymbol{x'}, \tag{1.4}$$

where G is the Green's function giving the stream function at $\boldsymbol{x}$ induced by a point source at $\boldsymbol{x'}$,

$$G(\boldsymbol{x}-\boldsymbol{x'}) = -\frac{1}{4\pi|\boldsymbol{x}-\boldsymbol{x'}|}, \tag{1.5}$$

in an unbounded domain and for the three-dimensional Laplacian in (1.1). For a system of N point vortices of strength $\kappa_j = (4\pi)^{-1}\iiint_{\mathcal{B}_j} q(\boldsymbol{x})\mathrm{d}^3\boldsymbol{x}$, and located at $\boldsymbol{x}_j$, $1 \le j \le N$, where $\mathcal{B}_j$ is a ball containing the point vortex i only, the PV field is

$$q(\boldsymbol{x}) = 4\pi \sum_{j=1}^{N} \kappa_j\, \delta(\boldsymbol{x}-\boldsymbol{x}_j). \tag{1.6}$$

Here $\delta()$ is the Dirac distribution. The stream function is therefore

$$\varphi(\boldsymbol{x}) = -\sum_{j=1}^{N} \frac{\kappa_i}{|\boldsymbol{x}-\boldsymbol{x}_j|}, \quad \forall \boldsymbol{x} \neq \boldsymbol{x}_j,\, 1 \le j \le N, \tag{1.7}$$

and the velocity is

$$\boldsymbol{u} = (u,v,0) = \left(-\frac{\partial\varphi}{\partial y}, \frac{\partial\varphi}{\partial x}, 0\right) = \sum_{j=1}^{N} \frac{\kappa_j(-y+y_j, x-x_j, 0)}{|\boldsymbol{x}-\boldsymbol{x}_j|^3}. \tag{1.8}$$

When applying the above formula to the location of point vortex k, one simply removes the spurious infinite self-induced contribution for $j = k$ from the sum (see the discussion in [39]). In a reference frame rotating uniformly at the angular velocity Ω about the vertical axis, the relative velocity $\boldsymbol{u'}$ is simply

$$\boldsymbol{u'} = \boldsymbol{u} - \Omega(-y, x, 0). \tag{1.9}$$

1.2. The problem's general geometry

We consider arrays of $N = 2n$ or $N = 2n+1$ vortices. The first set of n vortices is located along a horizontal ring of radius r_e at height z_e. The vortices are located at the azimuthal angles $\theta_j = 2(j-1)\pi/n$, $1 \le j \le n$ and have equal strength κ_e. A second set of n vortices is located along a horizontal ring of radius r_i at height z_i. The vortices are located at azimuthal angles $\theta_j = (2(j-n-1)+1)\pi/n$, $n+1 \le j \le 2n$ and have equal strength κ_i. In the case the array contains a central vortex, the central vortex is located at $(0,0,z_0)$ and has strength κ_0. Fig. 1 shows a top view of the geometry for a vortex array containing a central vortex and with $n = 5$. We consider staggered vortex arrays with $n \ge 2$, hence $N \ge 4$. Four vortices is the minimum number of vortices for chaotic dynamics to be possible, in absence of external forcing.

Without loss of generality, we set $z_e = 0$, $r_e = 1$ and $\kappa_e = 1$. We take $r_i \le r_e$, and $z_i \ge 0$. We denote $\Delta = z_i - z_e$ the vertical gap between the two rings. The full interaction depends on

(a) n, the number of vortices along each ring,

(b) r_i/r_e, the radius ratio between the two rings,

(c) Δ, the vertical offset between the two rings,

(d) κ_0, the strength of the central vortex (the cases without central vortex can be seen as special cases $\kappa_0 = 0$),

(e) z_0, the height of the central vortex.

The parameter space is too large to consider a comprehensive investigation. We will therefore focus on a few cross-sections of the full parameter space.

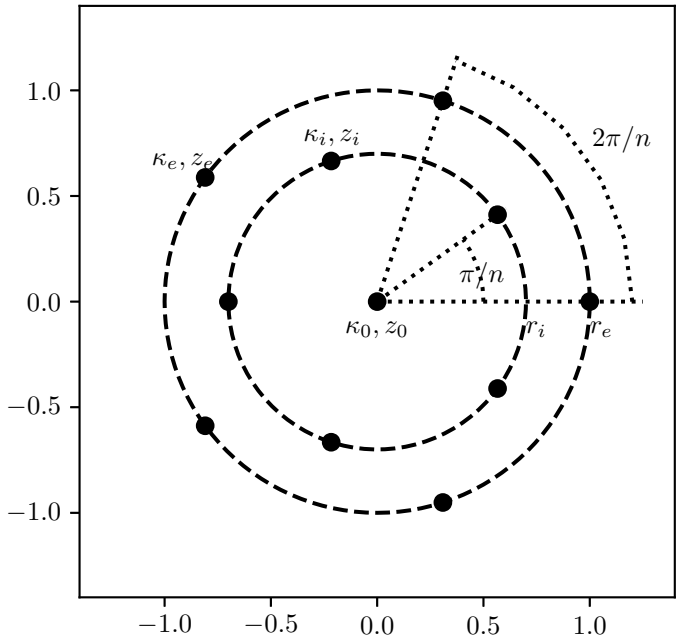

Fig. 1. Geometry of the vortex array for $N = 11\,(n = 5)$.

To find an equilibrium, we set values for n, Δ, r_i/r_e, z_0 and κ_0 and we determine κ_i so that the vortices on both rings rotate at the same angular velocity Ω. In practice this is done by expressing the angular velocity $|\boldsymbol{u}_1|/r_e$ of vortex 1 and the angular velocity $|\boldsymbol{u}_{n+1}|/r_i$ of vortex $n+1$ as functions of κ_i and equate the two velocities to obtain an explicit equation for κ_i. This, in turn, allows one to evaluate Ω. The vortex array is then in equilibrium (or steady) in a reference frame rotating uniformly at the angular velocity Ω. We also address the linear stability of the array with respect to vortex displacement modes

$$\boldsymbol{x}_i(t) = \boldsymbol{x}_i^{eq} + \hat{\boldsymbol{x}}_i e^{\sigma t}, \tag{1.10}$$

in the reference frame rotating at Ω. Here $\boldsymbol{x}_i^{eq}$ is the vortex location at equilibrium, while $\hat{\boldsymbol{x}}_i = (\hat{x}_i, \hat{y}_i, 0)$ is the horizontal perturbation mode (amplitude) and $\sigma = \sigma_r + \mathrm{i}\sigma_i \in \mathbb{C}$ is the mode's complex growth rate. The real part σ_r of σ is the actual growth rate while its imaginary part σ_i is its frequency. The perturbed locations are substituted into (1.9) where $\boldsymbol{u}$ is replaced by the linearised form of (1.8). This leads to an eigenvalue problem of size $2N$ where σ is an eigenvalue and $\hat{\boldsymbol{x}}$ is an eigenvector. This approach has been used in [35, 40]. All numerical codes are written in Fortran and the eigenvalue problem is solved using the standard Lapack library.

2. EQUILIBRIA AND LINEAR STABILITY

2.1. Vortex arrays without a central vortex: $N = 2n$

We first consider cases without a central vortex. To that purpose we explicitly remove the central vortex rather than setting $\kappa_0 = 0$. If we set $\kappa_0 = 0$ and retain a passive vortex located at $(0, 0, z_0)$,

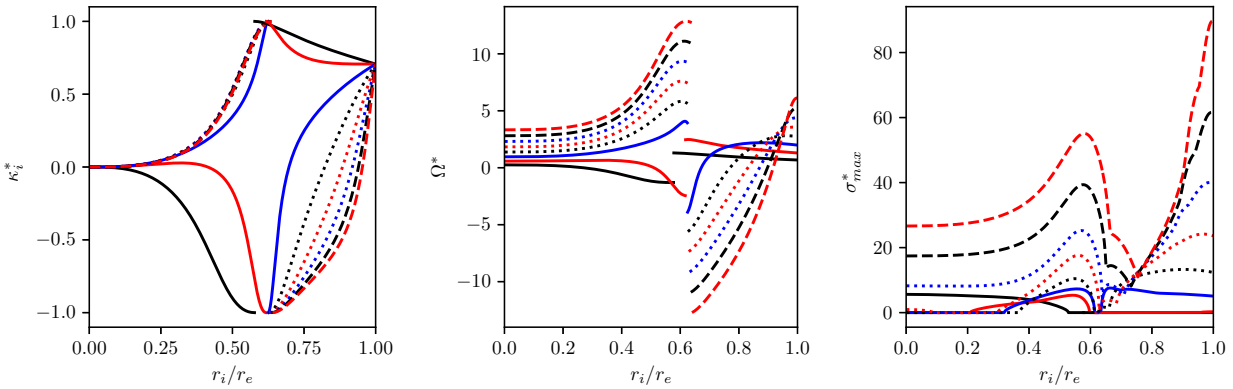

Fig. 2. Normalised strength κ_i^* (left), normalised equilibrium rotation velocity Ω^* vs r_i/r_e (middle), and normalised maximum growth rate σ^*_{max} (right) vs the radius ratio r_i/r_e for vortex arrays with no central vortex ($q_0 = 0$), $\Delta = 0$ and for $n = 2$ (solid black), $n = 3$ (solid red), $n = 4$ (solid blue), $n = 5$ (dotted black), $n = 6$ (dotted red), $n = 7$ (dotted blue), $n = 8$ (dashed black), $n = 9$ (dashed red).

the stability analysis could pick up spurious unstable modes for the passive particle which neither affect the vortex array nor the flow dynamics.

We start by considering the case $\Delta = 0$ where the two vortex rings of n vortices are co-planar. The arrays contain $N = 2n$ vortices in total. We study eight families of equilibria for $2 \leq n \leq 9$. For each value of n, we vary the radius of the inner ring in the range $0 < r_i/r_e \leq 1$, considering 1000 equally-spaced values. As mentioned above, we first determine κ_i so that the vortices are in mutual equilibrium, then we deduce Ω. We define a pseudo-time scale τ

$$\tau = \frac{1}{\sqrt{\kappa_e^2 + \kappa_i^2}} \tag{2.1}$$

and from this we define the normalised strength κ_i^* and the normalised rotation velocity Ω^*

$$\kappa_i^* = \tau\,\kappa_i, \quad \Omega^* = \tau\,\Omega \tag{2.2}$$

Strictly speaking τ does not have the dimension of a time since the strengths κ have the dimension of a volume integrated vorticity. But since we have taken $r_e = 1$, τ plays the role of a time scale in the problem.

Results for κ_i^* and Ω^* are summarised in Fig. 2. Results show that $\kappa_i^* \to 0$ as $r_i/r_e \to 0$ and $\kappa_i^* \to 1/\sqrt{2} \iff \kappa_i \to \kappa_e$ as $r_i/r_e \to 1$ for all values of n considered. The limiting case $r_i/r_e \to 1$ is simply the single ring of $2n$ vortices of equal strength, as expected. It should also be noted that the problem degenerates at $r_i = 0$ as all vortices of the inner ring converges to a single (central) vortex. In this case, the system is an equilibrium for any arbitrary strength of the single central vortex. We also see that there exists a critical radius r_c for the inner ring, which depends on n and for which no equilibrium is possible. Indeed $\kappa_i^* \to \pm 1$ as $r_i \to r_c^-$ and $\kappa_i^* \to \mp 1$ as $r_i \to r_c^+$. For $n \leq 3$, $\kappa_i^* \to -1$ (resp. $+1$) as $r_i \to r_c^-$ (resp. r_c^+) while it is the reverse for $n \geq 4$.

The detailed dependence of κ_i^* on r_i is however non trivial. For $n = 2$ and $r < r_c \simeq 0.578\,r_e$, $\kappa_i^* < 0$ and decreases monotonically as r_i increases. The vortices of the two rings are opposite-signed. For $r > r_c$, $\kappa_i^* > 0$ and also decreases monotonically as r_i increases, and the vortices of the two rings are like-signed. For $n = 3$, $\kappa_i^* \to 0^+$ as $r_i \to 0$. It increases to a local maximum of $\kappa_i^* \simeq 2.8 \times 10^{-2}$ at $r_i \simeq 0.319\,r_e$ as r_i increases before decreasing and reaching negative values for $0.413\,r_e < r_i < r_c \simeq 0.617\,r_e$. For $r_i > r_c$, $\kappa_i^* > 0$ and decreases monotonically as r_i increases. For $n \geq 4$ the situation changes. The vortex normalised strength κ_i^* first increases with $r_i \leq r_c$, with $r_c(n = 4) \simeq 0.624\,r_e$, $r_c(n = 5) \simeq 0.625\,r_e$, $r_c(n = 6) \simeq 0.628\,r_e$, $r_c(n = 7) \simeq 0.631\,r_e$, $r_c(n = 8) \simeq 0.635\,r_e$, $r_c(n = 9) \simeq 0.639\,r_e$. The values of the critical radius r_c are summarised in Table 1. We observe that r_c weakly depends on n, only slightly increasing as n increases. Then κ_i^* increases again as r_i increases for $r_i > r_c$. The normalised strength κ_i^* is first negative, with $\kappa_i^* \to -1$ as $r_i \to r_c^+$,

n	2	3	4	5	6	7	8	9
$\Delta = 0$	0.578	0.617	0.624	0.625	0.628	0.631	0.635	0.639
$\Delta = 0.2$	0.588	0.636	0.649	0.655	0.661	0.666	0.672	0.678
$\Delta = 0.4$	0.621	0.692	0.727	0.754	0.778	0.802	0.831	0.879
$\Delta = 0.8$	0.739	0.903	-	-	-	-	-	-

Table 1. Relative critical inner ring radius r_c/r_e for $2 \leq n \leq 9$ and $\Delta = 0$, 0.2, 0.4 and 0.8.

then it becomes zero for some $r_p < r_e$ which depends on n, and it is positive for $r_i > r_p$. Again the threshold r_p increases monotonically with n. The global rotation rate of the system Ω^* is strongly correlated to the strength of the vortices on the inner ring and follows a similar tendency as shown in Fig. 2.

The linear stability of the vortex arrays is complicated. We define the normalised growth rates

$$\sigma^* = \tau\, \sigma_r. \tag{2.3}$$

The maximum normalised growth rate σ^*_{max} of the vortex displacement modes is also shown in Fig. 2. For $n = 2$, the array is unstable for $r_i < 0.528\, r_e$. In this range the vortices lying along the inner ring have moderate (in magnitude) negative normalised strength $-0.963 < \kappa_i^* < 0$. It should be noted that $\kappa_i^* = -0.963$ corresponds to $\kappa_i/\kappa_e \simeq -3.57$. The system becomes stable for $r_i > 0.528\, r_e$. In particular we recover, for $r_i/r_e = 1$, the result that a single ring of four vortices is stable [35]. It should also be noted that the arrays are stable in the vicinity of $r_i = r_c$. For $n = 3$, the situation is different. The array is stable for $r_i < 0.21\, r_e$ for which the vortices of the inner ring have a small positive strength. The array is unstable for $0.21\, r_e \leq r_i < 0.597\, r_e$. There is a secondary narrow region of weak instability in the range $0.602\, r_e \leq r_i \leq 0.613\, r_e$. The equilibria are however stable for r_i in the near vicinity of r_c. Finally, the equilibria are also unstable for $0.96\, r_e \leq r_i \leq r_e$. We recover that the single ring of six vortices is indeed unstable [35]. For $n = 4$, the array is stable for $r_i < 0.32\, r_e$, a region where the vortices of the inner ring have a strength $0 < \kappa_i^* < 0.0903$. The array is then unstable for $0.32\, r_e \leq r_i < 0.614\, r_e$ and for $r_i > 0.624\, r_e$. We recover for $r_i = r_e$ that the single ring of eight vortices is unstable [35]. The narrow range of stable arrays for $0.614\, r_e \leq r_i \leq 0.624\, r_e$ corresponds to arrays with relatively intense positive strength vortices on the inner ring $\kappa_i^* > 0.953$. For $n = 5$, the arrays are stable for $0.37\, r_e < r_i$ where $0 < \kappa_i^* < 0.166$. The arrays are unstable for $0.37\, r_e \leq r_i < 0.612\, r_e$. As for the case $n = 4$, there is a very narrow region of stability of intense strength inner ring vortices for $0.613\, r_e < r_i < 0.627\, r_e$. The arrays are unstable for $r_i \geq 0.627\, r_e$. For $n = 6$, the arrays are unstable for $r_i \leq 0.087\, r_e$ for which the vortices in the inner ring have very low normalised strength, $0 < \kappa_i^* < 1.752 \times 10^{-3}$. The arrays are then stable for $0.087\, r_e < r_i < 0.299\, r_e$, then unstable for $r_i \geq 0.299\, r_e$. For $n = 7$, 8, 9 all arrays are unstable.

We next briefly discuss the modes of instability affecting the vortex arrays. The vortex displacement $\hat{\boldsymbol{x}}_i$ for the most amplified mode is shown in Fig. 3 for $r_i = 0.5\, r_e$ and various values of n. Recall that, since $\sigma \in \mathbb{C}$, the displacement $\hat{\boldsymbol{x}}_i = (\hat{x}_i, \hat{y}_i, 0) \in \mathbb{C}^3$ in general. In all cases, the modes instability are associated with vortices being moved away from its equilibrium position (a stationary point in the reference frame rotating with the configuration). It is therefore related to the topology of the local strain and shear exerted at the stationary points by the vortices. For $n = 2$ the most unstable mode has a growth rate $\sigma_{max} = \sigma_r \in \mathbb{R}$. The vortex displacement mode, also real, does not coincide with a global rotation nor a global translation and disrupt the equilibrium by making the vortices move relatively to each other. For $n = 3$ and $r_i = 0.5\, r_e$ the most amplified mode also corresponds to a real eigenvalue $\sigma_{max} = \sigma_r$. The displacement mode mostly affects the vortices of the inner ring whose strengths are $\kappa_i \simeq -0.167\, \kappa_e$, and make them mode outward (or inward, depending on the sign of the perturbation). For $n = 4$, 6, 8, where the number of vortices along each ring is even, the most unstable mode corresponds to the staggering of the vortices of the inner ring, see Fig. 3. It should be noted that the staggering of the vortices along a single ring of vortices is commonly observed for circular vortex arrays, see [35] and [36].

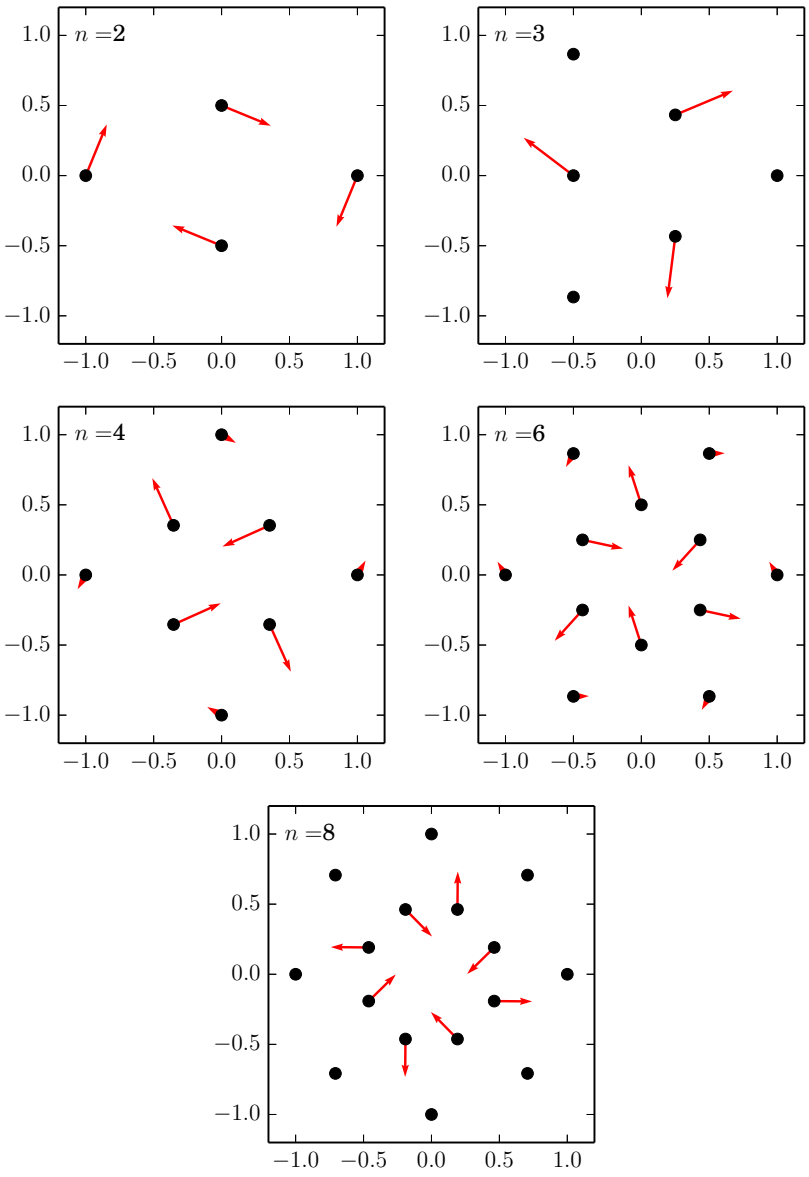

Fig. 3. Description of the most unstable displacement mode for vortex arrays without central vortex. $\Delta z = 0$ and $r_i = 0.5\, r_e$ is all cases. The number n of vortices in the array is indicated in each panel. The black bullets indicate the location $\boldsymbol{x}_i^{eq}$ of the point vortices while the red arrow show the most unstable displacement mode $\hat{\boldsymbol{x}}_i$ (real in these cases).

For odd values of n the situation may be more complex as shown in Fig. 4 for $n = 9$. First it should be noted that there are numerous unstable modes for any value of r_i/r_e (see the right panel of Fig. 4 for $n = 9$). The growth rates σ of the modes appear as pairs of complex conjugate eigenvalues. For $r_i/r_e = 0.5$ the complex conjugate pair of modes corresponding to the most amplified mode corresponds to a global rotation. The second most amplified mode mostly affects the vortices of the inner array, disrupting the relative equilibrium. For larger r_i/r_e the most amplified mode mostly affects the inner ring, again disrupting the relative equilibrium. Qualitatively, similar results are obtained for $n = 5$ and $n = 7$ (not shown).

We next briefly compare the stability properties of the three-dimensional QG arrays with the ones of planar two-dimensional ones. To that purpose, and using similar techniques we have first determined the equilibrium states for the arrays and studies their linear stability. Fig. 5 gives σ^*_{max} for the planar, two-dimensional vortex arrays. Qualitatively the results are very similar except for

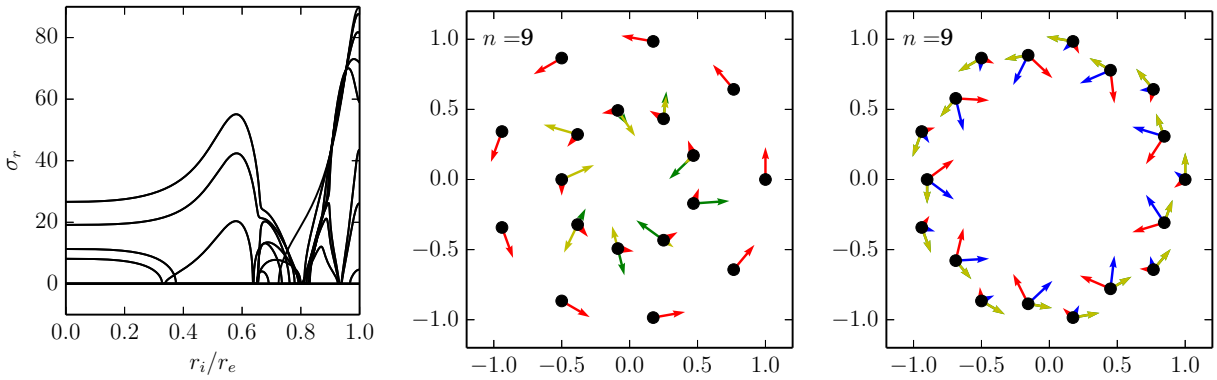

Fig. 4. Instability modes for $\Delta z = 0$, $n = 0$ and no central vortex vs r_i/r_e. Growth rates σ_r vs r_i/r_e (left panel). Displacement modes for $r_i/r_e = 0.5$ (middle panel) and $r_i/r_e = 0.9$ (right panel). The black bullets indicate the location $\boldsymbol{x}_i^{eq}$ of the point vortices while the arrows show the real part (red) and imaginary part (blue) of the displacement modes $\hat{\boldsymbol{x}}_i$ for the pair of complex conjugate modes with the largest growth rate σ_r. Same for the mode with the second largest growth rate with the green (real part) and yellow (imaginary part) arrows.

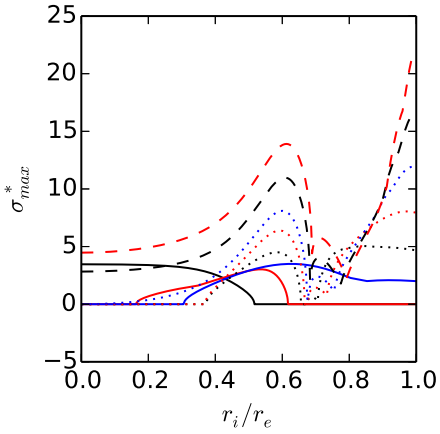

Fig. 5. Normalised maximum growth rate σ^*_{max} vs the radius ratio r_i/r_e for the planar, two-dimensional staggered vortex arrays without central vortex, and for $n = 2$ (solid black), $n = 3$ (solid red), $n = 4$ (solid blue), $n = 5$ (dotted black), $n = 6$ (dotted red), $n = 7$ (dotted blue), $n = 8$ (dashed black), $n = 9$ (dashed red).

the fact that the regions of stability are slightly shifted. In particular, as already pointed out by [35], for $r_i = r_e$ and $n = 3$, the planar, two-dimensional vortex array is stable while its QG counter-part is unstable.

Going back to the QG vortex arrays, we next investigate the influence of Δ on the characteristics of the equilibria and on their stability properties. We first look in detail at families of equilibria for three values of the vertical offset $\Delta/r_e = 0.2$, 0.4 and 0.8 before providing an overview in a larger parameter space for $\Delta/r_e \in [0, 1]$. Results for κ_i^*, Ω^* and σ^*_{max} are presented in Fig. 6 for $\Delta = 0.2\,r_e$, in Fig. 7 for $\Delta = 0.4\,r_e$, and finally in Fig. 8 for $\Delta = 0.8\,r_e$. Again, none of these arrays contains a central vortex. For $\Delta = 0.2\,r_e$, the qualitative trends are the same as for $\Delta = 0$. The main difference is a slight shift of r_c to a larger value for each n, see Fig. 6 and Table 1. We can also notice an overall reduction of the normalised rotation velocity Ω^*, associated with the decrease in the interaction intensity between the rings. This is due to their vertical separation, see Fig. 6 (middle panel). The qualitative structure of the unstable regions remains similar to the one for $\Delta = 0$ apart from a couple of noticeable differences. For $n = 3$, the small region of instability for $r_i \simeq r_e$, observed for $\Delta = 0$ disappears for $\Delta = 0.2\,r_e$. Again, this can be related to the weakening of the interaction between the two rings. The same is true for the narrow secondary region of

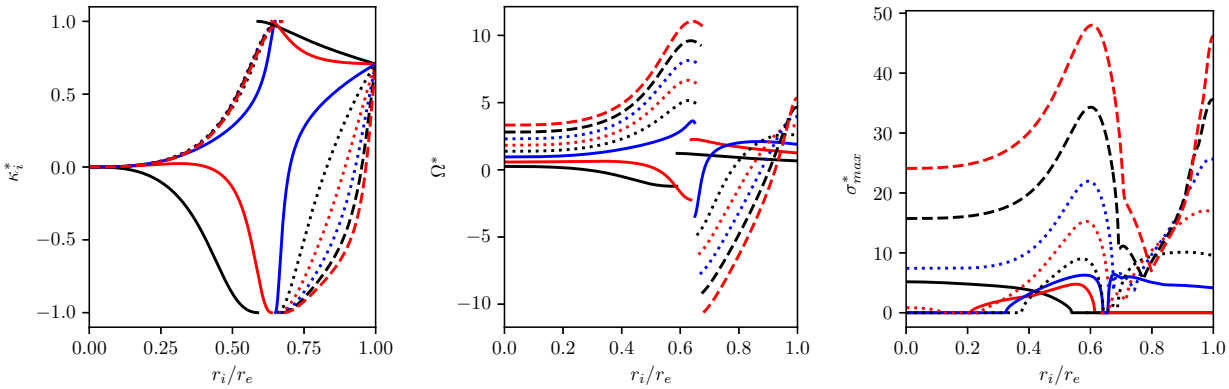

Fig. 6. Normalised strength κ_i^* (left), normalised equilibrium rotation velocity Ω^* vs r_i/r_e (middle), and normalised maximum growth rate σ^*_{max} (right) vs the radius ratio r_i/r_e for vortex arrays with no central vortex ($q_0 = 0$), $\Delta = 0.2$ and for $n = 2$ (solid black), $n = 3$ (solid red), $n = 4$ (solid blue), $n = 5$ (dotted black), $n = 6$ (dotted red), $n = 7$ (dotted blue), $n = 8$ (dashed black), $n = 9$ (dashed red).

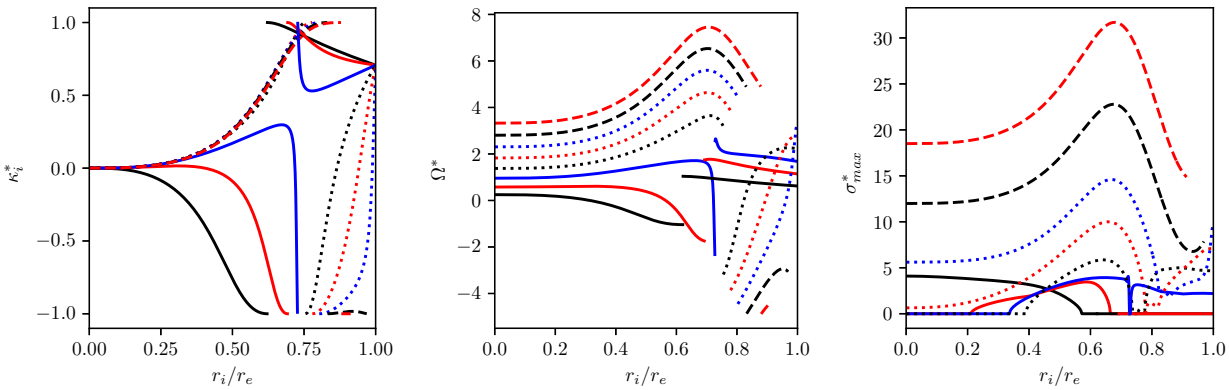

Fig. 7. Normalised strength κ_i^* (left), normalised equilibrium rotation velocity Ω^* vs r_i/r_e (middle), and normalised maximum growth rate σ^*_{max} (right) vs the radius ratio r_i/r_e (right) for vortex arrays with no central vortex ($q_0 = 0$), $\Delta = 0.4$ and for $n = 2$ (solid black), $n = 3$ (solid red), $n = 4$ (solid blue), $n = 5$ (dotted black), $n = 6$ (dotted red), $n = 7$ (dotted blue), $n = 8$ (dashed black), $n = 9$ (dashed red).

instability observed in the range $0.602\,r_e \le r_i \le 0.613\,r_e$ for $\Delta = 0$. No such region is found for $\Delta = 0.2\,r_e$. For $n = 4$, the narrow region of stable equilibria for $0.641\,r_e \le r_i \le 0.656\,r_e$, located between the the main regions of unstable arrays is slightly wider that the equivalent one observed for $\Delta = 0$ and occurs in a range of slightly larger radii. This is associated with the shift of r_c to a larger value. The qualitative differences for the other values of n are less noticeable. The limits in r_i separating the regions of stability/instability are slightly shifted towards higher values of r_i and the growth rates of the modes are marginally smaller when $\Delta \neq 0$. Increasing Δ further to $\Delta = 0.4\,r_e$ leads to more substantial differences from the arrays having $\Delta = 0$. The values of r_c increase, see Fig. 7 and Table 1, and overall the normalised rotation velocity Ω^* and the normalised growth rates σ^*_{max} are smaller. The most striking differences are $\kappa_i^*(r_i/r_e)$ and $\Omega^*(r_i/r_e)$ for $n = 4$. Now $\kappa_i^* \to -1$ as $r_i \to r_c^-$ and $\kappa_i^* \to 1$ as $r_i \to r_c^+$. The opposite occurs for $\Delta = 0$ and for $\Delta = 0.2$. This means that the sign of the strength of the vortices along the inner ring has changed compared to the cases with lower Δ in the vicinity of r_c. The behaviour of κ_i^* for both $r_i \to 0$ and $r_i \to 1$ however remains qualitatively similar to the previous cases. A second qualitative difference is the appearance of two further discontinuous changes in κ_i^* as a function of r_i/r_e for $n = 8$ and 9. For $n = 8$, $\kappa_i^* \to -1$ ($\kappa_i < 0$ and $|\kappa_i| \gg \kappa_e$) as $r_i/r_e \to 0.969^-$ and $\kappa_i^* \to 1$ ($\kappa_i \gg \kappa_e$) as $r_i/r_e \to 0.969^+$. For $n = 9$ the same behaviour happens around $r_i/r_e \simeq 0.913$. In both cases, we still recover $\kappa_i^* \to 1/\sqrt{2}$ as $r_i \to r_e$. For $\Delta = 0.8\,r_e$, more qualitative differences are observed. First, the curves $\kappa_i^*(r_i/r_e)$ are continuous

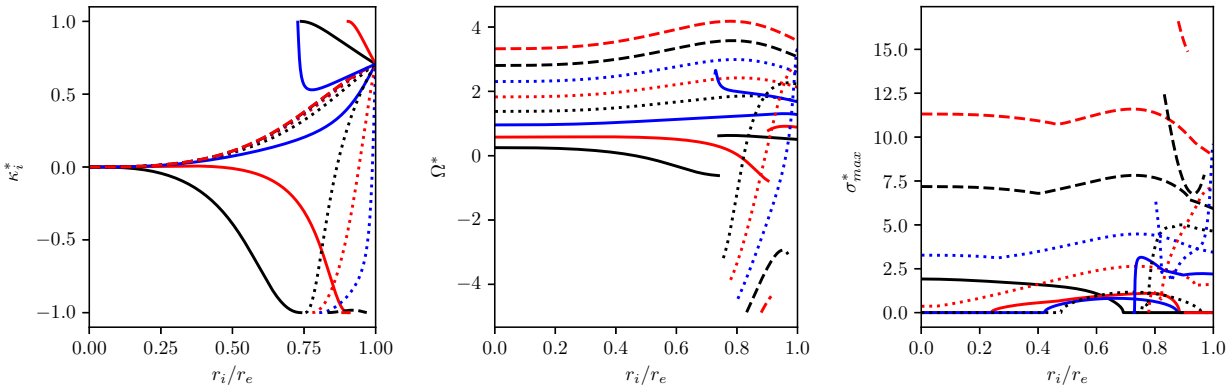

Fig. 8. Normalised strength κ_i^* vs the radius ratio r_i/r_e (left) and the normalised equilibrium rotation velocity Ω^* vs r_i/r_e (right) for vortex arrays with no central vortex ($q_0 = 0$), $\Delta = 0.8$ and for $n = 2$ (solid black), $n = 3$ (solid red), $n = 4$ (solid blue), $n = 5$ (dotted black), $n = 6$ (dotted red), $n = 7$ (dotted blue), $n = 8$ (dashed black), $n = 9$ (dashed red).

in the full range $[0, 1]$ for $n \geq 4$. This is the result of the continuous increase of r_c as Δ is increased. For $n = 4$, this implies the disappearance of the region of instability observed for smaller Δ for $r_i > r_c$. It also means that the very narrow region of stability observed for $r_i \to r_c^-$ for smaller Δ also disappears.

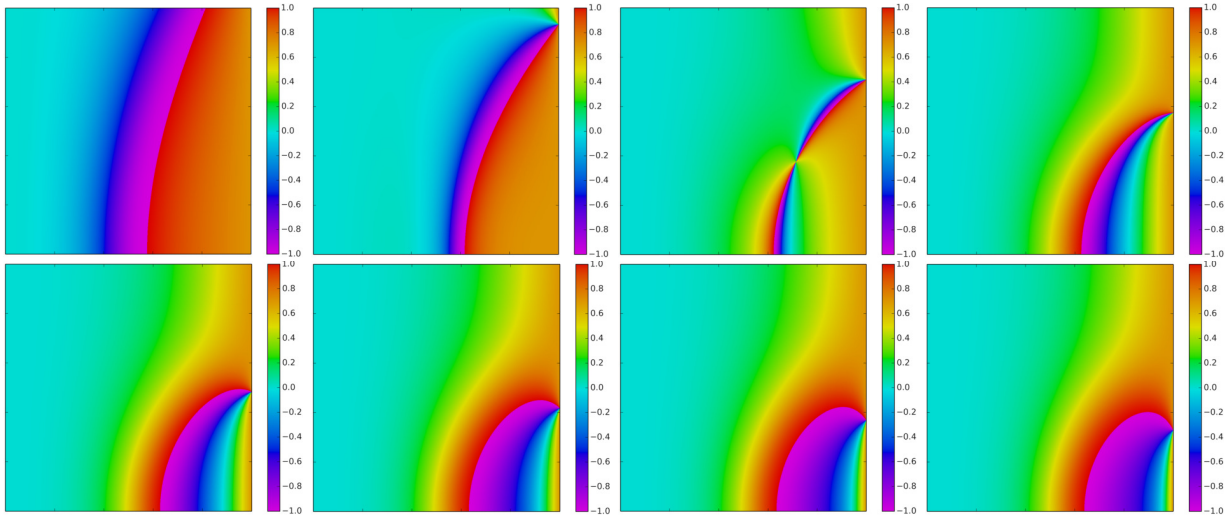

Fig. 9. Normalised strength κ_i^* for vortex arrays without central vortex in the plane $(r_i/r_e, \Delta)$ for $r_i/r_e \in [0, 1]$ and $\Delta/r_e \in [0, 1]$. From left to right then first row to second row: $n = 2$, 3, 4, 5, 6, 7, 8 and 9.

We finally provide a complete overview of the characteristics of the vortex arrays without a central vortex by providing the full fields $\kappa_i^*(r_i/r_e, \Delta)$ for $0 \leq r_i/r_e \leq 1$ and $0 \leq z_i/r_e \leq 1$, using 1000 uniformly-spaced values for both parameters, in Fig. 9, $\Omega^*(r_i/r_e, \Delta)$ in Fig. 10 and σ_{max}^* in Fig. 11. The figures confirm the general trends analysed above by detailing the four cross-sections for fixed values of Δ.

2.2. Vortex arrays with a central vortex: $N = 2n + 1$

We next investigate the influence of the addition of a central vortex on the characteristics of the equilibria and on their linear stability. The introduction of a central vortex adds two parameters: its strength κ_0 and its height z_0. A comprehensive analysis of the full parameter space $(n, r_i/r_e, \Delta, q_0, z_0)$ is out of reach.

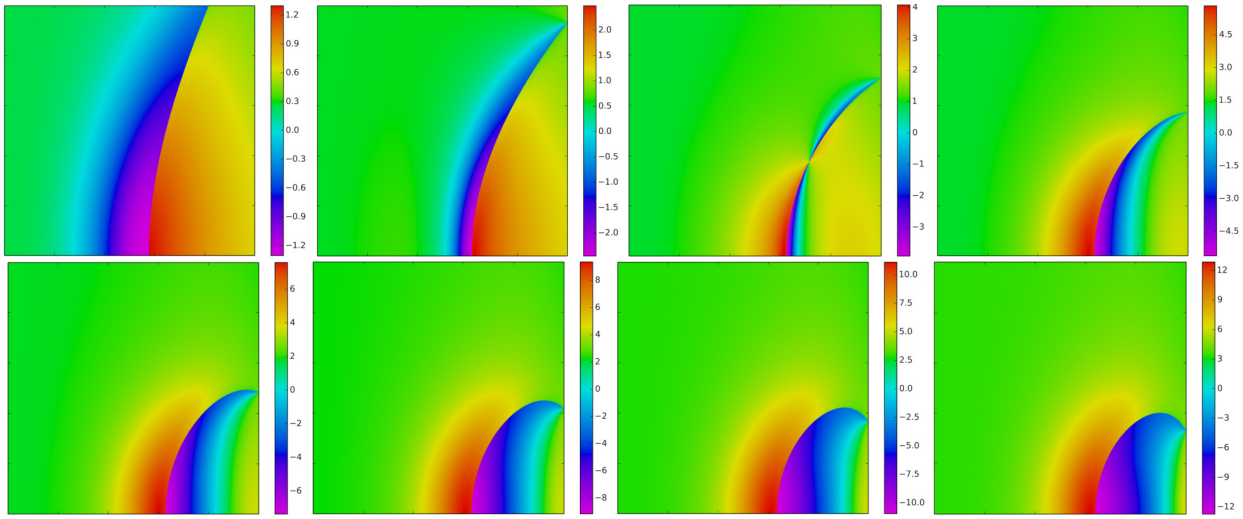

Fig. 10. Normalised rotation velocity Ω^* for vortex arrays without central vortex in the plane $(r_i/r_e, \Delta)$ for $r_i/r_e \in [0,1]$ and $\Delta/r_e \in [0,1]$. From left to right then first row to second row: $n = 2$, 3, 4, 5, 6, 7, 8 and 9.

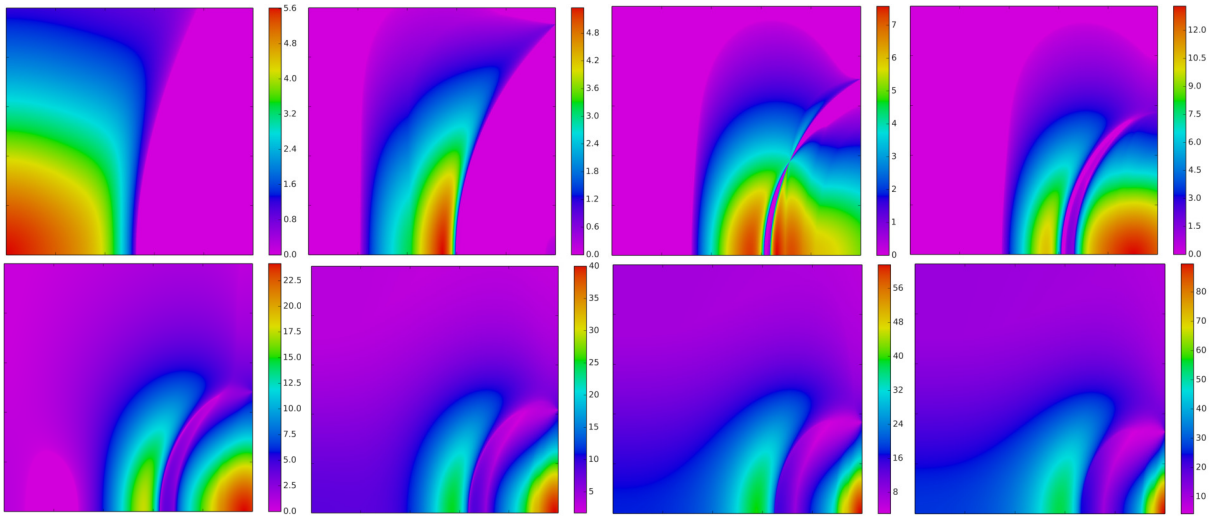

Fig. 11. Normalised maximum growth rate σ^*_{max} for vortex arrays without central vortex in the plane $(r_i/r_e, \Delta)$ for $r_i/r_e \in [0,1]$ and $\Delta/r_e \in [0,1]$. From left to right then first row to second row: $n = 2$, 3, 4, 5, 6, 7, 8 and 9.

For simplicity, we restrict attention to vortex arrays with $\Delta = 0$ in the rest of the section. We start by considering vortex arrays with $z_0 = 0$ and $\kappa_0/\kappa_e = 0.5$ and we vary $0 \le r_i/r_e \le 1$ for $2 \le n \le 9$. Results are presented in Fig. 12. First, it should be noted that the location (or existence) of the critical radius r_c remains unchanged as it does not depend on the central vortex. The central vortex however modifies κ_i^* and Ω^* by affecting the rotation of both rings. It also affects the stability of the rings, as already shown for a single ring [13, 35, 37]. First, we see that $\lim_{r_i \to 0} \kappa_i^* \neq 0$. But we recover $\lim_{r_i \to r_e} \kappa_i^* = 1/\sqrt{2}$, corresponding to a single ring of $2n$ equal-strength vortices. The presence of the positive strength vortex also changes the sign of κ_i^* for $n = 4$ and small r_i. The stability properties of the vortex arrays are also changed. The family of equilibria for $n = 2$ is unstable over a wider range of r_i compared to the case with no central vortex. For $n = 3$ the region of instability starts from $r_i \to 0$, with $\lim_{r_i \to 0} \sigma^*_{max} = 0$ in contrast with case without a central vortex for which the region of small r_i is stable. We should note however that the sign of the vortices in the inner ring is different in the two cases. For $n \ge 4$, the array is strongly unstable for small r_i with much larger σ^*_{max} compared to the array without a central vortex. The introduction of

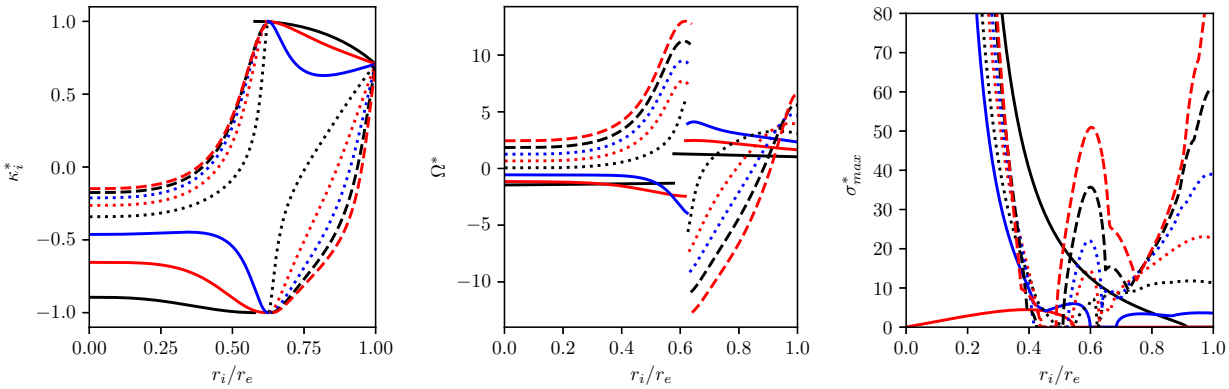

Fig. 12. Normalised strength κ_i^* vs the radius ratio r_i/r_e (left) and the normalised equilibrium rotation velocity Ω^* vs r_i/r_e (right) for vortex arrays with $\Delta = 0$, a central vortex at $z_0 = 0$ and strength $\kappa_0 = \kappa_e/2$ and for $n = 2$ (solid black), $n = 3$ (solid red), $n = 4$ (solid blue), $n = 5$ (dotted black), $n = 6$ (dotted red), $n = 7$ (dotted blue), $n = 8$ (dashed black), $n = 9$ (dashed red).

a central vortex has created a wider range of stable arrays for intermediate radii, $0.6 \leq r_i/r_e \leq 0.685$ for $n = 4$. It has also created small stable regions for larger n. For example, even for $n = 9$ the arrays for $0.436 \leq r_i/r_e \leq 0.488$ are stable, while all equilibria for $n = 9$, $\Delta = 0$ and no central vortex are unstable.

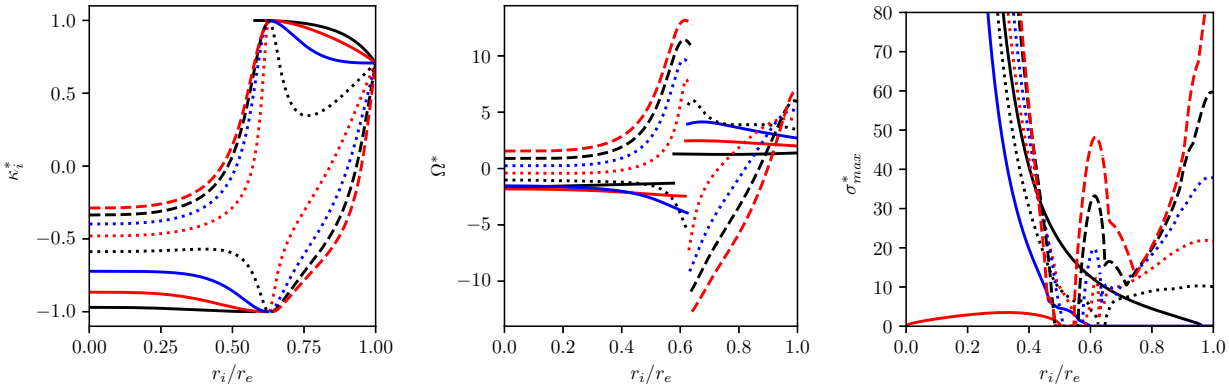

Fig. 13. Normalised strength κ_i^* vs the radius ratio r_i/r_e (left) and the normalised equilibrium rotation velocity Ω^* vs r_i/r_e (right) for vortex arrays with $\Delta = 0$, a central vortex at $z_0 = 0$ and strength $\kappa_0 = \kappa_e$ and for $n = 2$ (solid black), $n = 3$ (solid red), $n = 4$ (solid blue), $n = 5$ (dotted black), $n = 6$ (dotted red), $n = 7$ (dotted blue), $n = 8$ (dashed black), $n = 9$ (dashed red).

For $\kappa_0 = \kappa_e$, the trends are similar but accentuated. Results are presented in Fig 13. For $n = 9$, the range of r_i for which the array is stable is extended to $0.4485 \leq r_i/r_e \leq 0.547$, and is almost twice as wide as for $\kappa_0 = \kappa_e/2$. Note that the region of stability has also shifted toward larger r_i. For $n = 4$ all arrays are now stable for $r_i \geq 0.597$. On the other hand, the region of stability for $n = 2$ is drastically reduced, and stable arrays are only found for $r_i/r_e \geq 0.963$.

Changing the sign of the central vortex fundamentally changes the characteristics and the linear stability of the arrays. Results for $\kappa_0 = -\kappa_e$ are presented in Fig. 14. The normalised strength κ_i^* increases monotonically as r_i increases for all values of n considered, both for $r_i < r_c$ and $r_i > r_c$. As for the other cases, $\lim_{r_i \to r_e} \kappa_i^* = 1/\sqrt{2}$. We also note that $\kappa_i^* > 0$ for small r_i. The opposite is true in the two cases with $\kappa_0 > 0$ discussed previously. It should be noted however that the total vortex strength in the central region, obtained by adding the strength of the central vortex and the strengths of the vortices of the inner ring is not zero, even in the limit $r_i \to 0$. The stability properties of the arrays are also different and the regions of stability are typically smaller. For

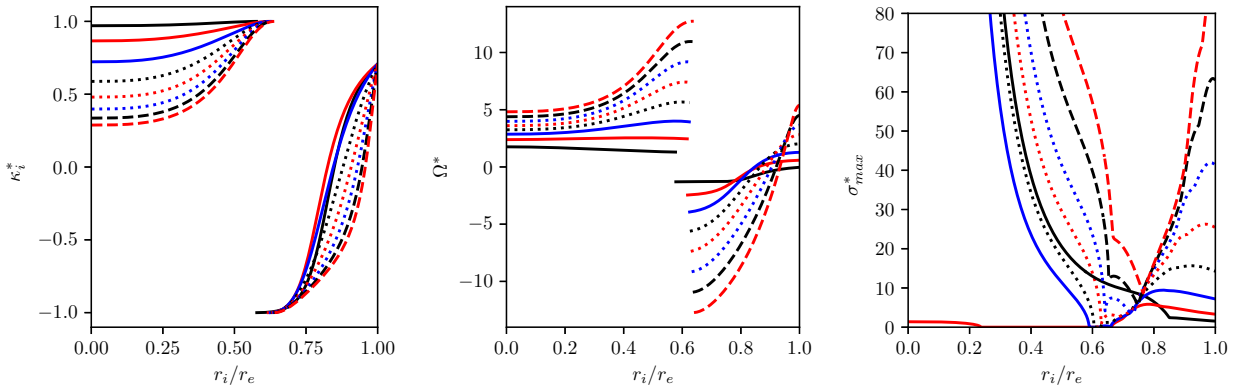

Fig. 14. Normalised strength κ_i^* vs the radius ratio r_i/r_e (left) and the normalised equilibrium rotation velocity Ω^* vs r_i/r_e (right) for vortex arrays with $\Delta = 0$, a central vortex at $z_0 = 0$ and strength $\kappa_0 = -\kappa_e$ and for $n = 2$ (solid black), $n = 3$ (solid red), $n = 4$ (solid blue), $n = 5$ (dotted black), $n = 6$ (dotted red), $n = 7$ (dotted blue), $n = 8$ (dashed black), $n = 9$ (dashed red).

example, all arrays for $n = 2$ are unstable. Moreover, in contrast with all other cases discussed for $\kappa_0 > 0$, the arrays for $n = 3$ are unstable as $r_i \to r_e$. Arrays with $n = 4$ and 5 have only a narrow region of stability of intermediate values of r_i/r_e. All arrays for $n \geq 6$ are unstable.

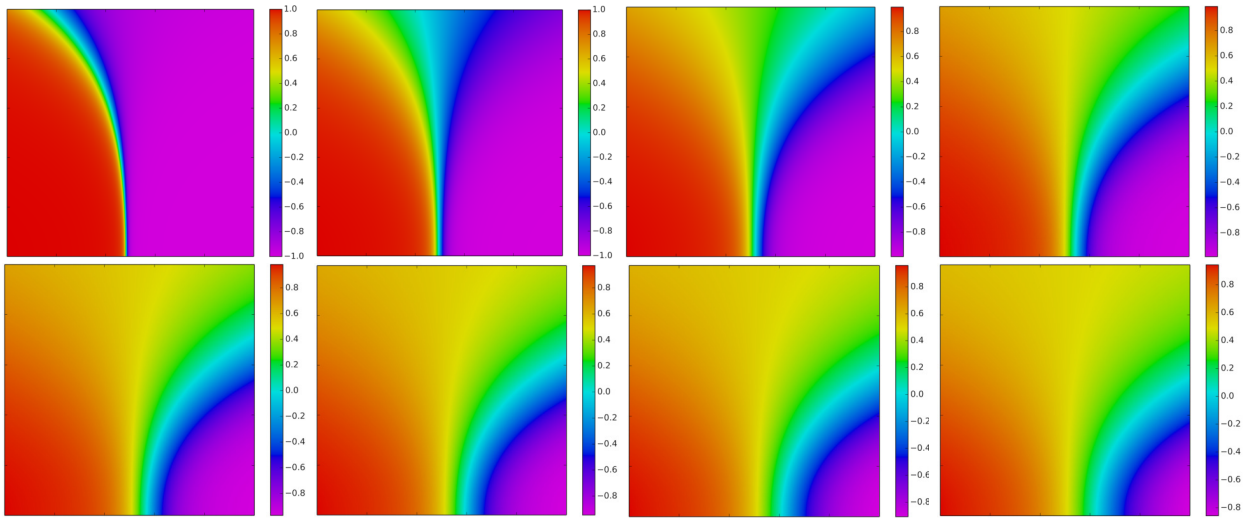

Fig. 15. Normalised strength κ_i^* for vortex arrays with a central vortex in the plane (q_0, z_0) for $q_0 \in [-5, 5]$ and $z_0/r_e \in [0, 1]$ when $\Delta = 0$ and $r_i/r_e = 0.5$. From left to right then first row to second row: $n = 2$, 3, 4, 5, 6, 7, 8 and 9.

We finally present an overview for two sets of families of equilibria with $\Delta = 0$ and for fixed r_i/r_e. Fig. 15 shows the normalised strength κ_i^* in the plane $(\kappa_0/\kappa_e, z_0/r_e)$ for $r_i/r_e = 0.5$. Fig. 16 shows the normalised rotation velocity Ω^* and Fig. 17 shows σ^*_{max} for the same equilibria. Similarly, Figs. 18, 19 and 20 show the same fields for $r_i/r_e = 0.8$. In both cases we consider 1000 values of κ_0/κ_e uniformly spaced between -5 and 5, and 1000 values of z_0/r_e uniformly spaced between 0 and 1. For $\Delta = 0$, the value $r_i = 0.5\, r_e$ is less than r_c while the value $r_i = 0.8\, r_e$ is larger than r_c, for all n considered. For all $r_i = 0.5\, r_e$ and all z_0, κ_i^* decreases as κ_0/κ_e goes from -5 to 5. As z_0 increases the amplitude of the variation decreases, indicating the weakening of the influence of the central vortex as it is moved away from the two rings. This appears to be more pronounced for large n. For larger n the vortices on the rings are closer together and interact more strongly together. Th central vortex has less relative influence. As expected, the trend for Ω^* is the same as it is closely linked to κ_i^*. For $n = 2$, the system is strongly unstable if the central vortex is intense ($|q_0|$ large) and close

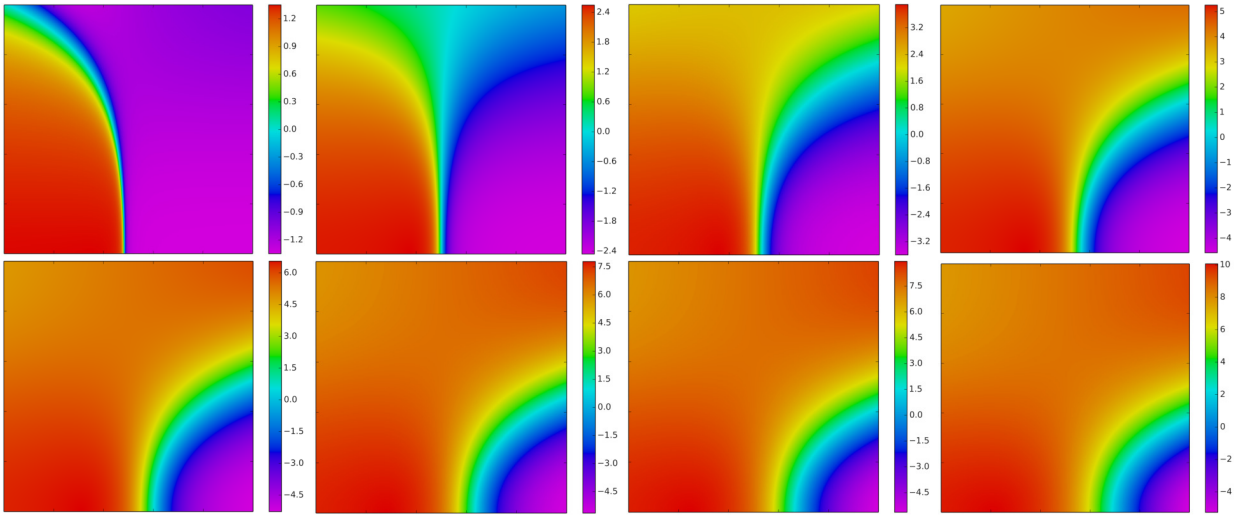

Fig. 16. Normalised rotation velocity Ω^* for vortex arrays with a central vortex in the plane (q_0, z_0) for $q_0 \in [-5, 5]$ and $z_/r_e \in [0, 1]$ when $\Delta = 0$ and $r_i/r_e = 0.5$. From left to right then first row to second row: $n = 2$, 3, 4, 5, 6, 7, 8 and 9.

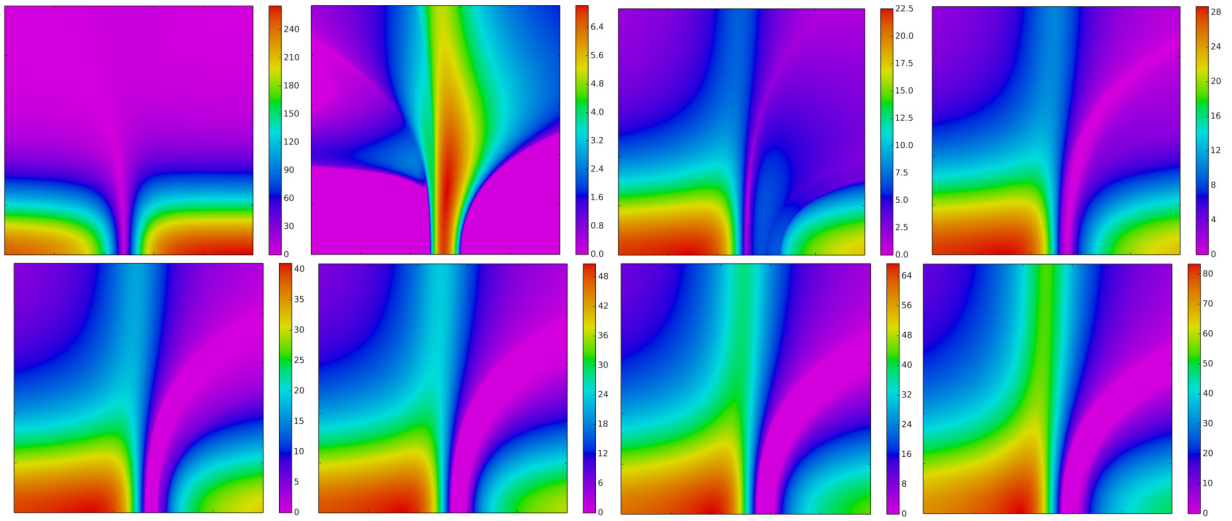

Fig. 17. Normalised maximum growth rate σ^*_{max} for vortex arrays without central vortex in the plane (q_0, z_0) for $q_0 \in [-5, 5]$ and $z_0/r_e \in [0, 1]$ when $\Delta = 0$ and $r_i/r_e = 0.5$. From left to right then first row to second row: $n = 2$, 3, 4, 5, 6, 7, 8 and 9.

to the horizontal plane of the rings (z_0 small). Stability and weak instability can be achieved for a weak central vortex or if the central vortex is located sufficiently far above the plane containing both rings. The situation changes for $n = 3$ where stability can be achieved for strong central vortex close to the rings. For $n \geq 4$, the linear stability of the arrays are qualitatively similar. Stability or weak instability is reached if the positive central vortex has a moderate influence on the ring. This is the case for small, positive κ_0 when z_0 is small and for increasing κ_0 as z_0 increases. In these cases the vortices on both rings are also positive. For $r_i/r_e = 0.8 > r_c/r_e$, the variation of κ_i^* vs κ_0 is reversed. It goes from negative values to positive values as κ_0/κ_e goes from -5 to 5. Again, the variation decreases as z_0 increases. Arrays of $n = 2$ vortices are unstable. For $n = 3$, stability is reached if κ_0 is larger than a negative threshold, which decreases as z_0 increases. For $n = 4$, arrays are stable if κ_0 is larger than a positive threshold which increases as z_0 increases. For $n = 5$, arrays can be stable for an intense central vortex close to the plane of the rings. All arrays are unstable for $n \geq 6$, at least within the range of parameters considered. Additional numerical experiments (not shown) indicate that stability can however be reached for in a finite range of larger $|\kappa_0|$.

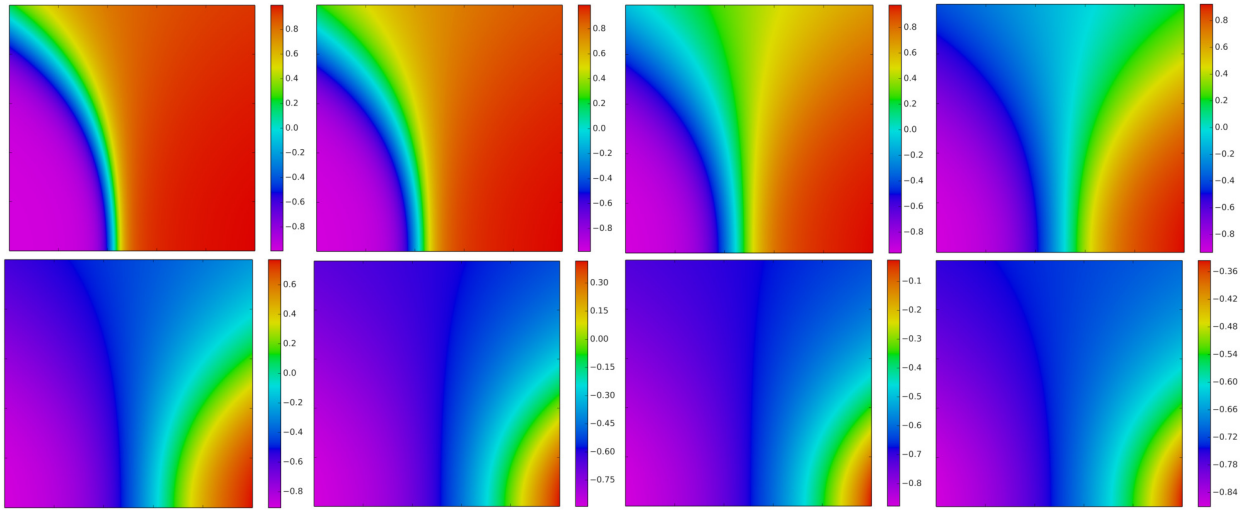

Fig. 18. Normalised strength κ_i^* for vortex arrays with a central vortex in the plane $(\kappa_0/\kappa_i, z_0/r_e)$ for $\kappa_0/\kappa_e \in [-5, 5]$ and $z_0/r_e \in [0, 1]$ when $\Delta = 0$ and $r_i/r_e = 0.8$. From left to right then first row to second row: $n = 2$, 3, 4, 5, 6, 7, 8 and 9.

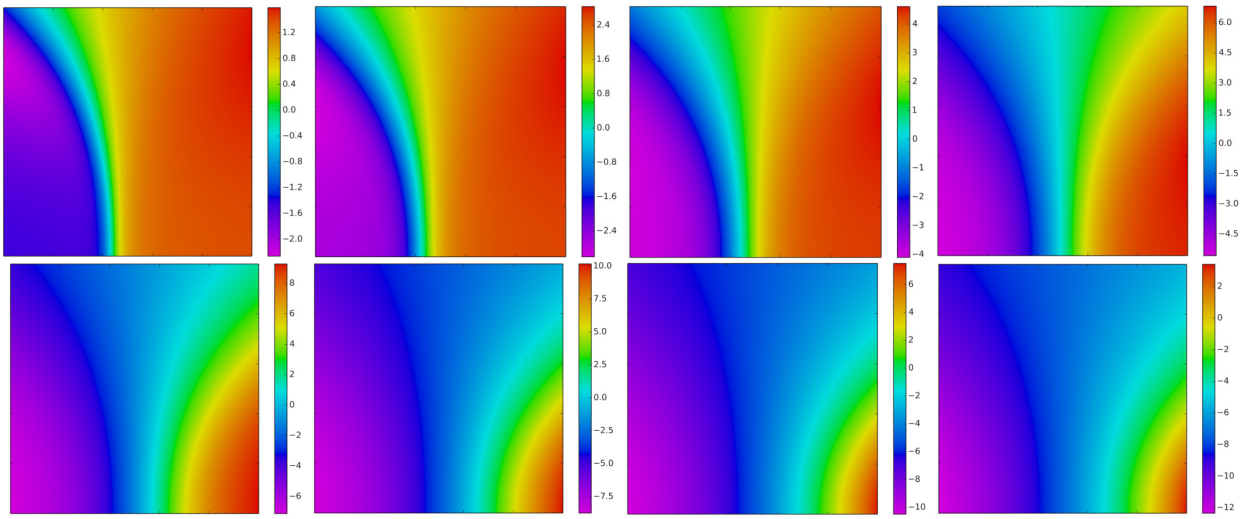

Fig. 19. Normalised rotation velocity Ω^* for vortex arrays with a central vortex in the plane $(\kappa_0/\kappa_e, z_0/r_e)$ for $\kappa_0/\kappa_e \in [-5, 5]$ and $z_0/r_e \in [0, 1]$ when $\Delta = 0$ and $r_i/r_e = 0.8$. From left to right then first row to second row: $n = 2$, 3, 4, 5, 6, 7, 8 and 9.

3. NONLINEAR EVOLUTION

We next show examples of the nonlinear evolution of unstable vortex arrays. Some comments on accuracy are presented in the Appendix. The vortex locations $\boldsymbol{x}_i$, $1 \le i \le N$ are marched in time using a fourth-order Runge-Kutta scheme. All trajectories are plotted in a reference frame uniformly rotating at the angular velocity Ω of the equilibrium. Hence for a stable equilibrium the vortices remain still. Perturbations are not imposed and they solely arise from the small numerical noise. This includes the finite accuracy of the value of κ_i^* for the equilibrium which is first determined numerically. We present a selection of cases where the vortices of the array have either a quasi-periodic or quasi-regular trajectories as well as cases where their motion appears to be chaotic. Recall that all arrays considered contain at least four vortices.

Fig. 21 shows the trajectories of the point vortices in the array with $\Delta = 0$ for $n = 2$, $r_i = 0.2\, r_e$ and no central vortex. The figure also shows the evolution of the distance $d_3 = |\boldsymbol{x}_3|$ between vortex 3, which belongs to the inner ring, and the origin. The equilibrium is unstable. There is first a transient phase where the vortices remain close to their equilibrium location. During this phase

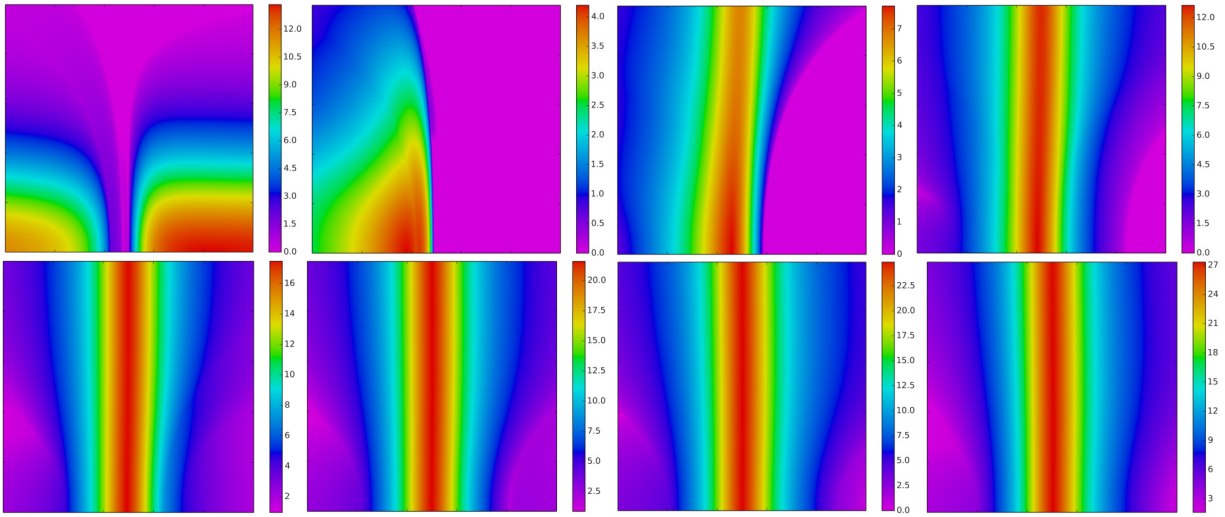

Fig. 20. Normalised maximum growth rate σ^*_{max} for vortex arrays without central vortex in the plane $(\kappa_0/\kappa_e, z_0/r_e)$ for $\kappa_0/\kappa_e \in [-5,5]$ and $z_0/r_e \in [0,1]$ whens $\Delta = 0$ and $r_i/r_e = 0.8$. From left to right then first row to second row: $n = 2$, 3, 4, 5, 6, 7, 8 and 9.

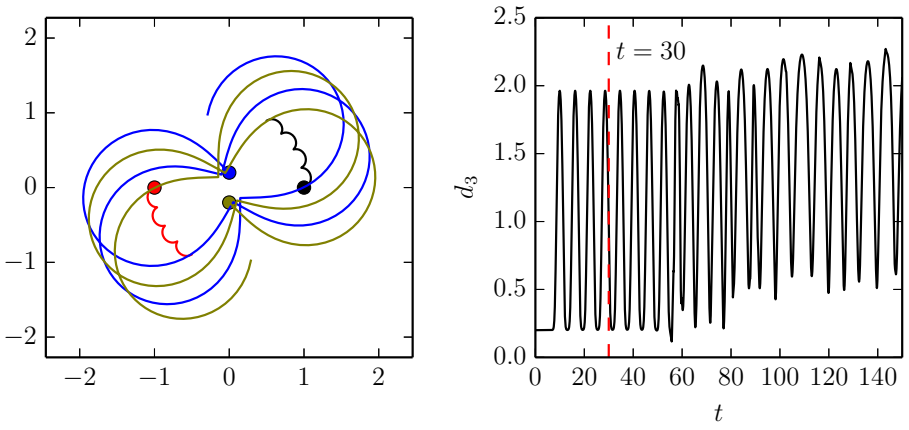

Fig. 21. Top view on the nonlinear evolution of the vortex array without central vortex and $\Delta = 0$ for $n = 2$, $r_i = 0.2\, r_e$, $t_{max} = 30$ (left). Distance $d_3 = |\boldsymbol{x}_3|$ vs time t for $0 \le t \le 150$ (right).

perturbations build up from the small numerical noise. Then the vortices commence a quasi-periodic motion, recovering periodically a near equilibrium configuration. Eventually, asymmetries build up from the numerical noise and the late time evolution becomes irregular as hinted by the evolution of d_3.

Fig. 22 shows the evolution of two other unstable arrays without a central vortex for $\Delta = 0$. The first array has $n = 3$ and $r_i/r_e = 0.5$. The three vortices of the inner ring first exchange location, with vortex 4 moving to the initial location of vortex 6, vortex 6 to the initial location of vortex 5 and vortex 5 to the one of vortex 4. This motion perturbs the rest of the array and all vortices move in a more convoluted pattern which becomes increasingly asymmetric. The second array has $n = 4$, and $r_i = 0.7\, r_e$. In this case the vortices of the inner ring have $\kappa_i \simeq 1.79 \times 10^{-2} \kappa_e$. This means that the vortices of the inner ring have a small strength in magnitude compared to the vortices of the outer ring and are almost passively advected. The vortices of the inner ring nearly move along the streamlines created by the strong outer vortex quartet, in the reference frame rotating with the equilibrium. The outer vortices slowly drift as a consequence of small perturbations induced by the moving weak inner vortices.

For comparison, we show the nonlinear evolution of equilibrium planar, two-dimensional vortex arrays for the same vortex numbers and same radius ratio r_i/r_e as the three examples detailed

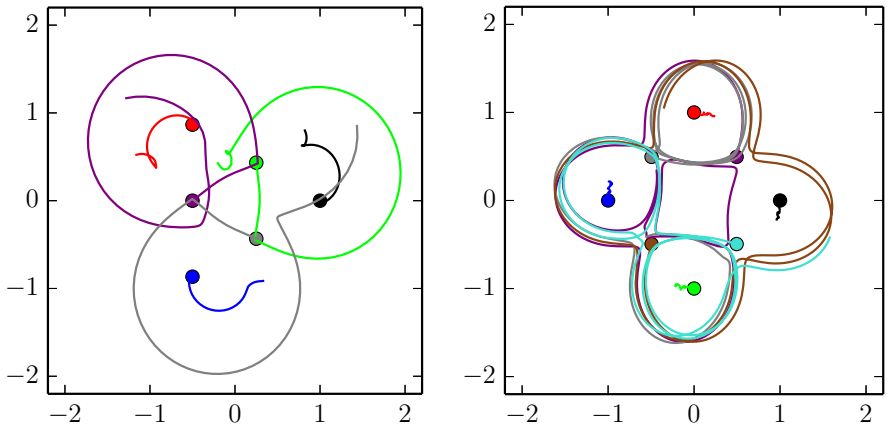

Fig. 22. Top view of the nonlinear evolution of vortex arrays without central vortex and $\Delta = 0$ for $n = 3$, $r_i/r_e = 0.5, t_{max} = 15$ (left) and for $n = 4$, $r_i = 0.7\, r_e$, $t_{max} = 15$ (right).

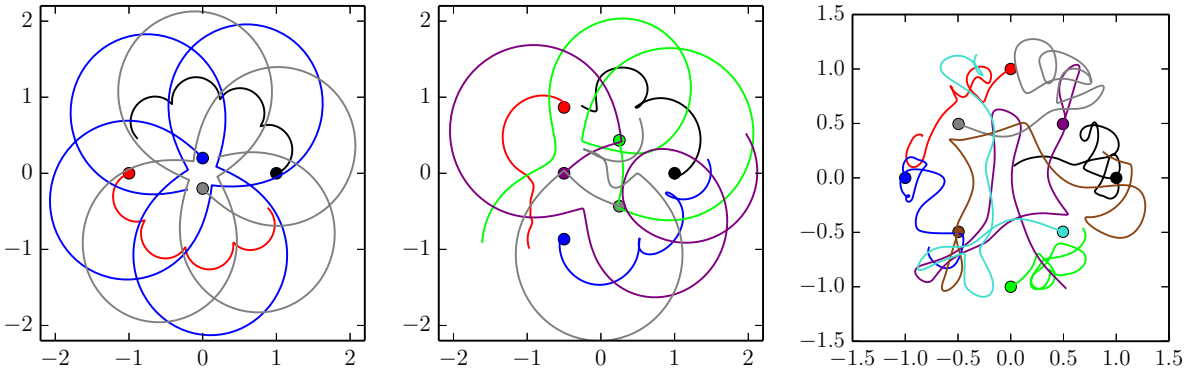

Fig. 23. View on the nonlinear evolution of planar, two-dimensional unstable arrays with no central vortex for $n = 2$ and $r_i/r_r = 0.2$ (left panel), $n = 3$ and $r_i/r_e = 0.5$ (middle panel) and $n = 4$ and $r_i/r_e = 0.5$ (right panel).

above. Note that however, since the Green's function is different, the strength ratios κ_i/κ_e and the background rotation Ω for the equilibria differ between the two-dimensional and the QG cases. Recall indeed that the velocity induced by a planar two-dimensional vortex (an infinite vortex line in the three-dimensional space) decays as the inverse distance between the vortex and the evaluation point while it is the distance squared in the QG case. Hence the configurations of planar, two-dimensional arrays and the QG arrays (with $\Delta = 0$) are not identical for a given n and r_i/r_e. For $n = 2$ and $r_i/r_e = 0.2$ the nonlinear evolution of the planar two-dimensional arrays and the QG arrays are qualitatively similar. The quasi-periodic quasi semi-circular trajectories of the vortices has radii of curvature smaller for the QG array than the ones for the planar two-dimensional array. The same is true for $n = 3$ and r_i/r_e. In both cases, the strength of the vortices of the inner ring is less, in magnitude, in the QG case compared to the one of the planar, two-dimensional case. For $n = 4$ and r_i/r_e the two-dimensional vortex array is more sensitive to chaotic dynamics.

Going back to the QG vortex arrays, Fig. 24 shows the chaotic motion of the vortices of the unstable array with $n = 5$, $\Delta = 0$, $r_i = 0.5\, r_e$ and no central vortex. The evolution of the distance $d_1 = |\boldsymbol{x}_1|$ confirms the erratic motion of the point vortices.

Figure 25 shows example of the chaotic motion of the vortices for three unstable vortex arrays with no central vortex and $n = 4$ and $\Delta = 0.2\, r_e$, $n = 5$ and $\Delta = 0.2\, r_e$, and finally $n = 9$ and $\Delta = 0.4\, r_e$. In all three cases $r_i = 0.5\, r_e$. For $n = 4$, the initial evolution conserves some symmetries. For the two other cases presented, with a larger, odd number of vortices along the rings, symmetries are broken early. Recall that these vortex arrays are typically sensitive to numerous unstable modes

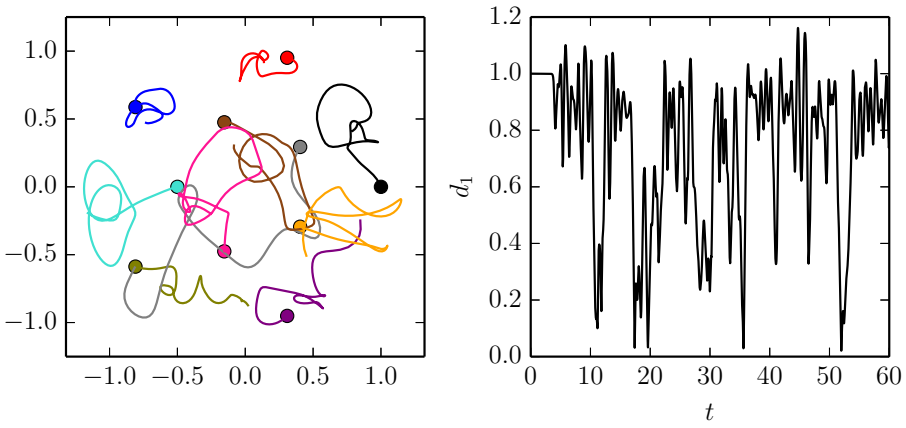

Fig. 24. Top view of the nonlinear evolution of the vortex array without central vortex and $\Delta = 0$ for $n = 5$, $r_i = 0.5\, r_e$, $t_{max} = 6.25$ (left). Distance $d_1 = |\boldsymbol{x}_1|$ vs time t for $0 \le t \le 60$ (right).

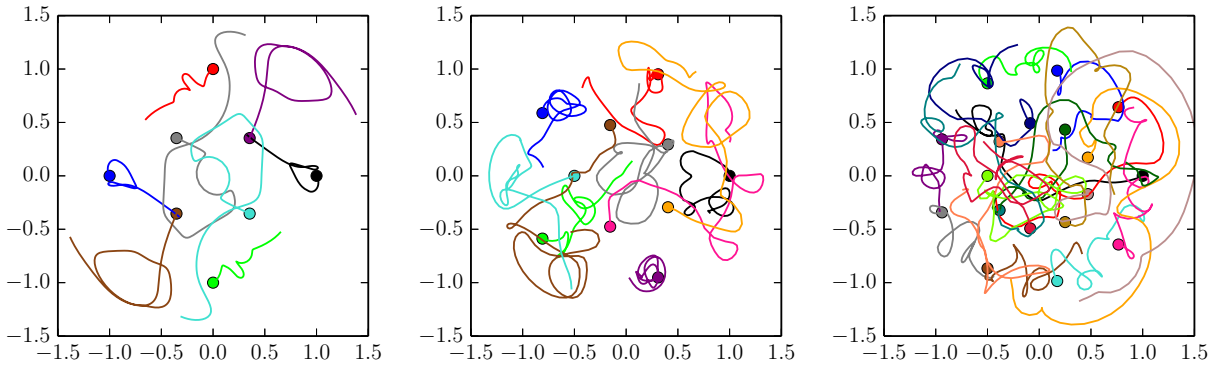

Fig. 25. Top view of the nonlinear evolution of the vortex array without central vortex and $\Delta = 0.2\, r_e$ and $r_i = 0.5\, r_e$ and for $n = 4$ (left) and $n = 5$(middle). The right panel shows the nonlinear evolution of the vortex array with $n = 9$ $r_i/r_e = 0.5$ and $\Delta = 0.4\, r_e$.

which can all compete. These examples show that, qualitatively, the same regimes of nonlinear motions can be observed in arrays with $\Delta \neq 0$.

We finally consider another case where the early evolution of the vortices exhibits a regular behaviour before becoming chaotic. We consider the unstable vortex array with a central vortex for $n = 9$, $\Delta = 0$, $r_i/r_e = 0.8$, $\kappa_0 = \kappa_e$, $z_0 = 0$. A top view of the vortex trajectories is shown in Fig. 26 while Fig. 27 shows the evolution of $d_1 = |\boldsymbol{x}_1|$. In this case, the vortices of the inner ring have strength $\kappa_i \simeq -0.92\, \kappa_e$. Hence the vortices of the two rings have an opposite strength of comparable magnitude. This provides the conditions for the formation of vortex dipoles. Indeed, the instability first makes each vortex of the inner ring move closer to one of the vortices of the outer ring, forming a vortex dipole. The dipoles then move away from the centre of the domain. The vortex dipoles reach an apogee at $t = 2.17$, see the right panel of Fig. 26 and Fig. 27. The vortex dipoles then converge back to the configuration in relative equilibrium, see the middle panel of Fig. 26 and Fig. 27. Then each inner vortex moves on the other side of an outer vortex while the outer vortex shifts one place in the array. Both motions are clockwise, see the right panel of Fig. 26. The latter sequence repeats three times, see Fig. 27. Then the vortices form dipoles again which move outward as indicated by the increase of d_1 in Fig. 27 from $t \gtrsim 5.5$. By the time the dipoles move back inward for $t \gtrsim 6.55$, asymmetries due to numerical noise have built up. The symmetry breaking eventually induces an erratic vortex motion (not shown).

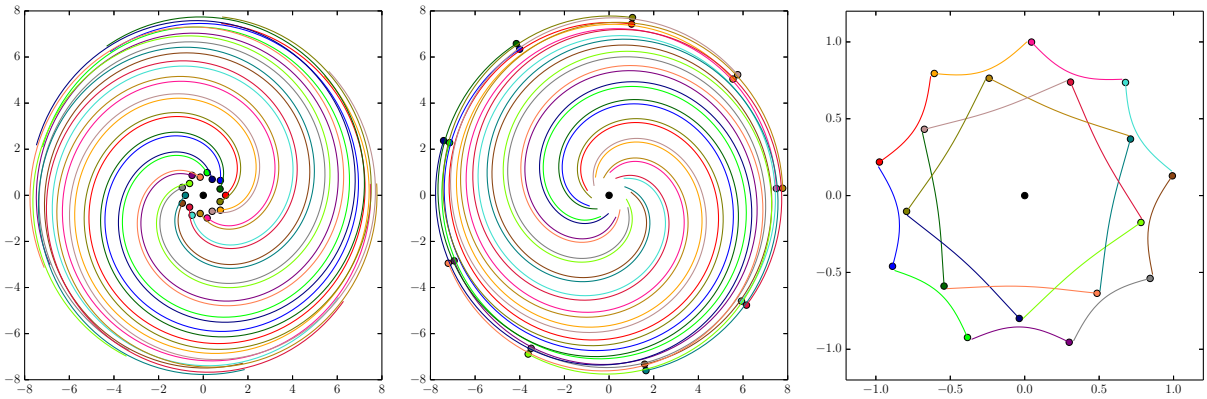

Fig. 26. Top view of the nonlinear evolution of the vortex array with a central vortex for $n = 9$, $\Delta = 0$, $r_i/r_e = 0.8$, $\kappa_0 = \kappa_e$, $z_0 = 0$. Trajectories for $0 \le t \le 21.7$ (left), $21.7 \le t \le 33$ (middle), $33 \le t \le 39.1$. In each panel the bullet indicates the starting location in the time window shown.

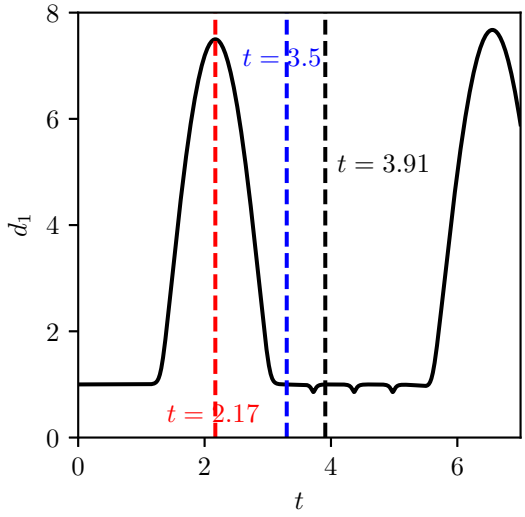

Fig. 27. Distance $d_1 = |\boldsymbol{x}_1|$ vs time t for the vortex array with a central vortex for $n = 9$, $\Delta = 0$, $r_i/r_e = 0.8$, $\kappa_0 = \kappa_e$, $z_0 = 0$.

4. CONCLUSIONS

We have determined relative equilibria for staggered vortex arrays in a dynamical regime relevant to the oceans. Some equilibria are stable, others are unstable. Our results however suggest that it is possible to find stable configurations for all numbers of vortices n especially if the array contains a central vortex. This may help to explain the apparent robustness of the staggered eight-vortex array ($n = 4$) having a central vortex observed over the north pole of Jupiter [41].

The nonlinear evolution of unstable arrays exhibits an extremely rich dynamics and deserves further investigation. Another natural extension of this work is to consider finite volume vortices and to investigate how the vortex deformation influences the evolution. Despite being a classical problem which has already been extensively studied in the literature, the dynamical richness offered by vortex arrays still provides new directions for future study.

APPENDIX. INVARIANTS AND ACCURACY

We briefly discuss the accuracy of the calculations. To that purpose, we verify that the flow invariants are respected within acceptable limits for the practical relevance of the discussion. Similarly to the classical planar, two-dimensional vortex dynamics, the QG vortex dynamics

conserves some fundamental invariants, namely the linear impulse $\boldsymbol{I}$, defined for a set of discrete point vortices as

$$\boldsymbol{I} = (I_x, I_y) = \sum_{i=1}^{N} \kappa_i \, (x_i, y_i), \tag{A.1}$$

the angular impulse

$$J = \frac{1}{2} \sum_{i=1}^{N} \kappa_i \, (x_i^2 + y_i^2), \tag{A.2}$$

and the interaction energy (which is also the Hamiltonian of the system)

$$H = \sum_{i=1}^{N} \sum_{j=i+1}^{N} \frac{\kappa_i \kappa_j}{|\boldsymbol{x}_i - \boldsymbol{x}_j|} \tag{A.3}$$

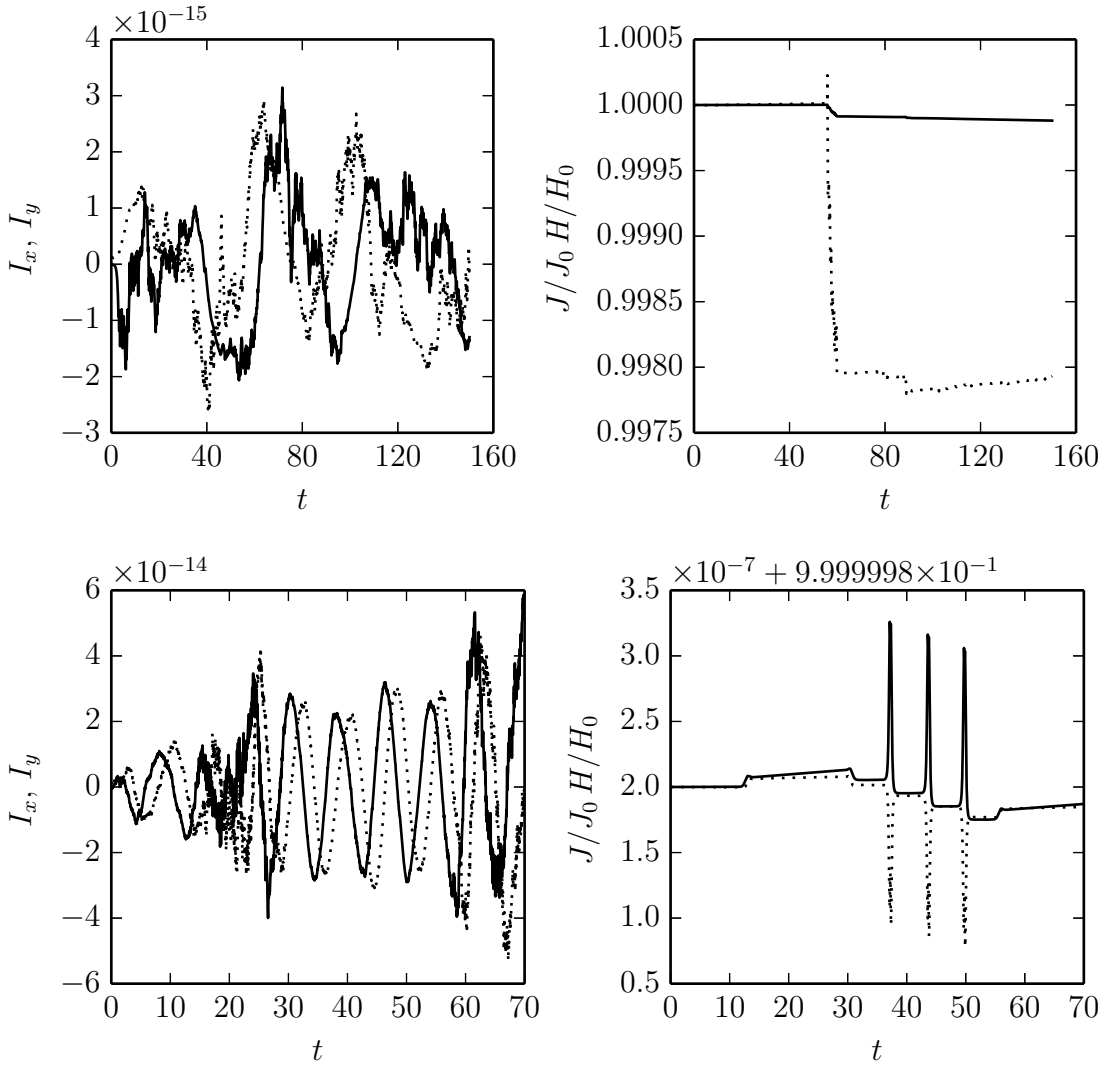

Fig. 28. Evolution of the linear impulse I_x, I_y and the scaled angular impulse J/J_0 and interaction energy H/H_0 for the case shown in Fig. 21 with $n = 2$ $\Delta z = 0$, $r_i/r_e = 0.2$ and no central vortex (top panels) and for $n = 9$, $r_i/r_e = 0.8$, and a central vortex $(\kappa_0, z_0) = (1, 0)$.

Figure 28 shows the evolution of the linear impulses I_x, I_y and of the scaled angular impulse J/J_0 and interaction energy H/H_0 for the case presented in Fig. 21 with $n = 2$, $\Delta = 0$, $r_i/r_e = 0.2$ and no central vortex (top panels) and for $n = 9$, $\Delta = 0$, $r_i/r_e = 0.8$, and a central vortex $(\kappa_0, z_0) = (1, 0)$ presented in Fig. 26. Here J_0 and H_0 are the initial values of the angular impulse and the interaction energy respectively. Results show that the linear impulse (initially zero by symmetry) is conserved within machine precision. Angular impulse J is conserved within 0.012% for the case with $n = 2$ while the energy is conserved with 0.2% for a time step $\Delta t = 0.075$ which is enough for the purpose of the discussion. In particular, for the initial evolution $t < 50$ (which includes the first phases of the non-trivial unstable evolution), accuracy is much higher. For $n = 9$ accuracy is higher as the time step used is smaller $\Delta t = 0.0025$ (the vortex velocities are larger in this case). Small errors are associated with the finite accuracy of the time integration, especially when some vortices get close together and their velocity increases. For long integration periods, these errors could be mitigated by using an adaptive time step. We are however only interested in the early evolution of the arrays.

CONFLICT OF INTEREST

The author declares that he has no conflicts of interest.

ACKNOWLEDGEMENT

The author wishes to thank David Dritschel for helpful discussions during the preparation of this paper.

REFERENCES

1. Helmholtz, H. von, Über Integrale der hydrodynamischen Gleichungen, welche der Wirbelbewegung entsprechen. *J. für die reine und angewandte Mathematik*, 1858, vol. 55, pp. 25–55.
2. Kirchhoff, G. R., *Vorlesungen über mathematische Physik. Mechanik*, Leipzig: Teubner, 1876.
3. Thomson, W., Vortex statics, *Proc. Roy. Soc. Edin.*, 1875, vol. 9, pp. 59–73.
4. Thomson, W., Floating magnets, *Nature*, 1878, vol. 18, pp. 13–14.
5. Mayer, A. M., On the Morphological Laws of the Configurations formed by Magnets floating vertically and subjected to the attraction of a superposed magnet; with notes on some of the phenomena in molecular structure which these experiments may serve to explain and illustrate, *Am. J. Sci.*, 1878, vol. 16, ser. 3, pp. 247-256.
6. Thomson, J. J., *A Treatise on the Motion of Vortex Rings*, London: MacMillan, 1883, pp. 94–108.
7. Havelock, T. H., The stability of motion of rectilinear vortices in ring formation, *Lond. Edin. Dubl. Phil. Mag. S. 7*, 1931, vol. 11(70) Suppl., pp. 617–633.
8. Morton, W. B., Vortex Polygons, *Proc. Roy. Irish Acad.: A. Maths. Phys.*, 1935, vol. 42 pp. 21–29.
9. Khazin, L. G., Regular polygons of point vortices and resonance instability of steady states, *Sov. Phys. Dokl.*, 1976, vol. 21(10), pp. 567–569.
10. Mertz, G. J., Stability of body-centered polygonal configurations of ideal vortices, *Phys. Fluids*, 1978, vol. 21(7), pp. 1092–1095.
11. Stewart, H. J., Periodic properties of the semi-permanent atmospheric pressure systems, *Quart. Appl. Math.*, 1943, vol. 1(3), pp. 262–267.
12. Stewart, H. J., Hydrodynamics problems arising from the investigation of the transverse circulation of the atmosphere, *Bull. Am. Math. Soc.*, 1945, vol. 51(11), pp. 781–799.
13. Morikawa, G. K. and Svenson, E. V., Interacting Motion of Rectilinear Geostrophic Vortices, *Physics of Fluids*, 1971, vol. 14(6), pp. 1058–1073.
14. Aref, H., Stability of relative equilibria of three vortices, *Phys. Fluids*, 2009, vol. 21, 094101.
15. Kizner, Z., Stability of point-vortex multipoles revisited, *Phys. Fluids*, 2011, vol. 23, 064104.
16. Kizner, Z., On the stability of two-layer geostrophic point-vortex multipoles, *Phys. Fluids*, 2014, vol. 26, 046602.
17. Kurakin, L. G. and Yudovich, V. I., The stability of stationary rotation of a regular vortex polygon, *Chaos*, 2002, vol. 12(3), pp. 574–595.
18. Kurakin, L. G. and Ostrovskaya, I. V., On Stability of Thomson's Vortex N-gon in the Geostrophic Model of the Point Bessel Vortices, *Regul. Chaotic Dyn.*, 2017, vol. 22(7), pp. 865–879.
19. Kurakin, L.G. and, Ostrovskaya, I.V. and Sokolovskiy M.A., On the stability of discrete tripole, quadrupole, Thomson's vortex triangle and square in a two-layer/homogeneous rotating fluid, *Regul. Chaotic Dyn.*, 2016, vol. 21(3), pp. 291–334.

20. Kurakin, L. and Melekhov, A. and Ostrovskaya, I., A survey of the stability criteria of Thomson's vortex polygons outside a circular domain, *Bol. Soc. Mat. Mex.*, 2016, vol. 22, pp. 733–744.
21. Kurakin, L.G. and Ostrovskaya, I.V. and Sokolovskiy, M.A., Stability of discrete vortex multipoles in homogeneous and two-layer rotating fluid , *Doklady Physics*, 2015, vol. 60(5), pp. 217–223.
22. Kurakin, L.G., Influence of annular boundaries on Thomson's vortex polygon stability , *Chaos*, 2014, vol. 14, 023105.
23. Kurakin, L.G., The stability of the steady rotation of a system of three equidistant vortices outside a circle , *J. of Appl. Math. and Mech.*, 2011, vol. 75(2), pp. 227–234.
24. Kurakin, L.G. and Ostrovskaya, I.V., Stability of the Thomson vortex polygon with evenly many vortices outside a circular domain , *Siberian Mathematical Journal*, 2010, vol. 51(3), pp. 463–474.
25. Kurakin, L.G. and Ostrovskaya, I.V., Nonlinear Stability Analysis of a Regular Vortex Pentagon Outside a Circle , *Regular and Chaotic Dynamics*, 2012, vol. 17(5), pp. 385–396
26. Kurakin, L.G., On the Stability of Thomson's Vortex Configurations Inside a Circular Domain , *Regular and Chaotic Dynamics*, 2010, vol. 15(1), pp. 40–58.
27. Kurakin, L.G., On stability of a regular vortex polygon in the circular domain , *J. Math. Fluid Mech.*, 2005, vol. 7. Suppl. 3, pp. S376–S386.
28. Kurakin, L.G., On nonlinear stability of the regular vortex systems on a sphere , *Chaos*, 2004, vol. 14(3), pp. 592–602.
29. Kurakin, L.G., Stability, resonances, and instability of regular vortex polygons in a circular domain , *Doklady Physics*, 2004, vol. 49(11), pp. 658–661.
30. Kizner, Z. and Khvoles, R. and McWilliams, J. C., Rotating multipoles on the f- and γ-planes, *Phys. Fluids*, 2007, vol. 19, 016603.
31. Dritschel, D. G., The stability and energetics of corotating uniform vortices *J. Fluid Mech.*, 1985, vol 157, pp. 95–134.
32. Crowdy, D. G., Exact solutions for rotating vortex arrays with finite-area cores, *J. Fluid Mach.*, 2002, vol. 469, pp. 209–235.
33. , Xue, B. B. and Johnson, E. R. and McDonald, N. R., New families of vortex patch equilibria for the two-dimensional Euler equations, *Phys. Fludis*, 2017, vol. 29, 123602.
34. Sokolovskiy, M. A. and Koshel, K. V. and Dritschel, D. G. and Reinaud, J. N., N-symmetric interaction of N hetons. Part I: Analysis of the case N=2, 2020, *Phys. Fluids*, vol. 32, 096601.
35. Reinaud, J. N., Three-dimensional quasi-geostrophic vortex equilibria with m-fold symmetry, *J. Fluid Mech.*, 2019, vol. 863, pp. 32–59.
36. Reinaud, J. N. and Dritschel, D. G., The stability and the nonlinear evoution of quasi-geostrophic toroidal vortices, *J. Fluid Mech.*, 2019, vol. 863, pp. 60–78.
37. Dritschel, D. G., Ring configurations of point vortices in polar atmospheres, *Regul. Chaotic Dyn.*, 2021, *under review.*
38. Vallis, G. K., *Atmospheric and Oceanic Fluid Dynamics*, Cambridge: Cambridge University Press, 2006.
39. Dritschel, D. G. and Boatto, S. The motion of point vortices on closed surfaces, *Proc. R. Soc. A*, 2015, vol. 471, 20140890.
40. Reinaud, J. N., Existence, stability and formation of baroclinic tripoles in quasi-geostrophic flows, *J. Fluid Mech.*, 2015, vol. 785, pp. 1–30.
41. Adriani, A. and Mura, A. and Orton, G. and Hansen, C. and Altieri, F. and Moriconi, M. L. and Rogers, J. and Eichstdt, G. and Momary, T. and Ingersoll, A. P. and Filacchione, G. and Sindoni, G. and Tabataba-Vakili, F. and Dinelli, B. M. and Fabiano, F. and Bolton, S. J. and Connerney, J. E. P. and Atreya, S. K. and Lunine, J. I. and Tosi, F. and Migliorini, A. and Grassi, D. and Piccioni, G. and Noschese, R. and Cicchetti, A. and Plainaki, C. and Olivieri, A. and O'Neill, M. E. and Turrini, D. and Stefani, S. and Sordini, R. and Amoroso, M., Clusters of cyclones encircling Jupiter's pole, *Nature*, 2018, vol. 555, pp. 216–219.